TECHNICAL NOTE: M-DT-N TN24-10

Transport Canada QVI

From: CLUE Project

Date: 2024-03-29

Revision 0

CLUE Project

Continuous Logging of Underwater noise Emissions
Final Report

Prepared by: CLUE Project

1 EXECUTIVE SUMMARY

The CLUE-project, Continuous Logging of Underwater noise Emissions, is a joint project initiated by ABB and DNV and funded by Transport Canada through the Quiet Vessel Initiative. Additionally, the project has also been made possible by Royal Caribbean Cruise Lines as they have made one of their vessels available for installation of the instrumentation and system setup that has been developed through the project. Royal Caribbean Cruise Lines have also assisted in facilitating the so-called calibration measurements required to develop the transfer functions to further substantiate the methodology suggested by the project.

The idea behind the project is a simplification of measurement procedures for underwater radiated noise from ships using pressure sensors as well as characterization of radiated noise from podded propulsion thrusters.

Through the project, a real-time tool has been developed to track the underwater noise emissions from a ship in operation.

Characterization of the noise emissions from the ABB Azipods has been achieved through the combination of different sensors that were installed near and inside the pod units. The instrumentation is discussed in detail in Chapter 6. The target ship is in operation, and was in dry-dock for a short period when the system was installed. Further considerations that were necessary to comply with the necessary requirements is discussed in Chapter 7 with regards to the system setup, while the installation is discussed in Chapter 8.

To calibrate the onboard system relative to what is experienced in the far field, a correlation study between simultaneous measurements onboard and offboard, using hydrophones in the water column, has been carried out. This test was done while the ship was in normal operation and for two operating conditions. The measurement results and the findings, together with considerations of simulations of magnetic underwater radiated noise (MURN) are presented in Chapter 10.

Chapter 9 includes discussions on findings from the measurement data within the installation period. Vast amounts of data have been gathered throughout the project. The measurement results can give new insights into the performance relative to underwater noise for cruise ships in general and ships equipped with podded propulsion systems in particular. Of high interest is especially the off-design conditions, as underwater from such ships is generally measured under specified controlled operating conditions, and not necessarily actual relevant operations such as manoeuvring in ports or other conditions with high requirements to the operability of the machinery.

The calibration measurements that were carried out showed in general good agreement between the measured levels by the pressure sensors close to the propeller and the hydrophones deployed in the water. Exceptions were a singing phenomenon around 60 – 80 Hz, as well as contributions from magnetic underwater radiated noise (MURN) in the range of ~250-500 Hz.

Based on the statistics derived from the dataset, it is suggested that a cavitation inception system should be based on statistical data, since the variability in instantaneous spectra is significant and will most likely end up in a large number in false positives and vice versa. Statistical data is believed to be a much more robust foundation for such an algorithm, and should be based on operational parameters where the correlation to whether or not it is cavitating is based on statistics from long term measurements.

One of the most important aspects of CLUE has been to demonstrate the feasibility of a live monitoring system for underwater radiated noise and also verifying the feasibility of measuring close to the source and the fact that controlling the noise and reducing the strength of the source results in reduced noise levels experienced by marine life.

It has also been shown that quite accurate far field URN predictions can be based on near field measurements augmented by a digital twin accounting for the significant electromagnetic noise components. The digital twin can possibly be used in the future to minimize the emitted noise from the drivetrain and thereby reducing the noise levels experienced in the far field.

2 ACKNOWLEDGEMENTS

The CLUE project, ABB and DNV, would like to extend its gratitude to Transport Canada and the Quiet Vessel Initiative for making the project possible through the funding of the project and also in assisting in defining and developing the project targets.

Also crucial for making the project possible was RCCL by making their vessel available for the system installation. It is great to see ship owners making efforts to make shipping more sustainable, and the CLUE project is eager to continue the collaboration. ABB and DNV would also specifically thank RCCL for facilitating full scale underwater noise hydrophone measurements.

3 INTRODUCTION

Underwater noise from human activities has in the last decade received considerable attention from an environmental perspective. Exposure to strong underwater noise from anthropogenic noise sources has been proven to cause evasive behaviour and increased stress on marine life forms. In the oceans, where the visibility is limited because of the efficient electromagnetic absorption properties of water, species like fish, whales and dolphins depend heavily on sound for communication, hunting and navigation over large distances. There's an indication that these behaviours are disrupted by the increase in human activity in the oceans and the subsequent generation of noise. This issue has started to draw more scrutiny from the scientific community, with researchers proposing that underwater noise could emerge as a notable concern, alongside climate change and pollution.

As a natural consequence of the increased attention on the impact of underwater noise on marine life, there has been an increased focus on documenting, controlling and reducing the contributions to underwater noise from human activity in the oceans. To facilitate this, it is vital to increase our understanding of the importance of various noise generating mechanisms to be able to mitigate the generated noise. It is furthermore important to quantify the contribution from a representative population of seagoing vehicles to quantify each individual's or group of vehicles' importance on a global scale to better understand how to effectively reduce the overall impact. As several of the noise generating mechanisms, strong enough to effectively contribute to the far field radiated noise, have a large theoretical complexity associated with them, a large part of the research is focused on measurements and characterization of acoustic signatures. Today, there are several available measurement methodologies varying in complexity. Most of which are time-consuming, costly and are only applicable to certain geographical areas. The latter because most standards rely on various assumptions and limitations with regards to for instance water depth, background noise, wave- and weather conditions.

The methodology proposed herein consists of onboard measurements and is motivated by several aspects. Firstly, by the need for a quick and cost saving solution for measurements with purpose of documenting a ship's underwater radiated noise. The primary sources onboard moreover seem to be localized in the near vicinity of the propellers with a rather predictable free field propagation characteristics from source to the far field. It is further believed that the current methodologies are impractical or financially inapplicable to some of the ship types that are presumably among the most substantial contributors to the radiated noise in the oceans. An unknown topic covered herein is also the variations in noise emissions in actual sailing conditions due to external as well as intended factors such as manoeuvring or power adjustments. Today, a similar measurement methodology exists which is described in the class guideline to DNV's Silent notation. It is only applicable to ship types where it is assumed that the propellers are the only potential sources onboard that may violate the respective underwater radiated noise criteria. This means that it is not a method generally suitable to accurately describe the far field acoustic signature, but it is intended to measure whether or not the propeller induced noise from the vessel is within a set of criteria greater than the potential noise generated by other sources onboard. One of the shortcomings is of course when unforeseen other factors, such as mechanical vibrations, contribute on a scale equivalent or higher than the noise from the propellers. In the near field, the acoustic mode shapes induced by such sources can be large in extent as well as complex. The pressure amplitude of such mode shapes can vary a lot and the resulting pressure one measures is highly depending on where the sensors are placed. Moreover, modes that are most prominent in some locations on the hull may be less important in the far field and vice versa, due to the radiation efficiency and directivity. To overcome such issues, the work carried out in this report will attempt to augment measurements of propeller noise onboard by corrections obtained by theoretical vibro-acoustical computations of noise induced by the propulsion electromotor. It is moreover believed that the source with the highest variability in source strength with respect to operating parameters and external factors is cavitation noise from the propellers. Under this assumption, one can use the methodology to estimate the noise emissions at all times, since the electromotor is believed to be covered by theoretical predictions whereas the variations in propeller source strength during a certain voyage is recorded at all times. By further assuming that the relation between the propeller source strength and the far field radiated noise can be described by a constant frequency dependent transfer function, it is possible to estimate the URN of the ship continuously as long as one has at least one set of measurements or a good prediction of the transfer function between the measured pressure on the hull and the observed sound pressure level in the far field.

4 PROJECT GOALS

The project goals and targets were summarized concisely in the Contribution Agreement for the project (ref. /1/), which again was based on the proposal document (ref. /2/) and the discussions leading up to the project kick-off.

4.1 Objective(s)

The main project goals include the development of a continuous measurement system for measuring propeller noise source levels, correcting them with vibro acoustic computations and measured transfer function, to enable monitoring of apparent far field underwater noise emissions from cavitation and electromagnetic noise; development of a high level environmental underwater noise monitoring tool. This tool may be treated as a proof of the concept that such systems work and may be scalable and more refined in the future and could support owners and/or regulators on minimizing shipping noise in the future.

The project has to a vast extent achieved what it set out to do; installation of a continuous measurement system onboard an operating ship, the transmission of measured onboard processed data and the onshore analysis of the data. Also of high value is the data itself and the increased understanding of the workings of the machinery components in its noise radiation.

4.2 Activities:

The activities carried out during the project was concisely specified in the project contribution agreement (ref. /1/) and is reiterated below.

Stage 1: Planning and preparation

- Conduct desktop studies (such as, identifying the data to be sent ashore, recording needs assessments, preliminary calculations of transfer function form electromotor, etc.)
- Determine required system specifications
- Setup and program required system specifications
- Determine which vessels will be utilized for a pilot of the continuous measurement unit

Stage 2: Project delivery (Proof of concept)

- Acquire equipment and components
- Setup trial (which can include preliminary setup of measurement system, testing of receiving data from the radio data system, testing of measurement processing, etc.)
- Process received data from the radio data system
- Implement source exposure level heatmap
- Implement cavitation inception detection system

Stage 3: Full-scale installation and vessel operation

- Install pressure sensor, sound analysers, loggers and radio data system
- Incorporate system in the radio data system
- Proceed with vessel sailing with operational equipment
- Test transmission of data packs with underwater noise levels using the radio data system
- Continuous updating of the system
- When available, run a correlation study between far-field results form a fixed hydrophone station and onboard measurements
- Development of progress reports
- Development of final report on Project results

5 THEORETICAL BACKGROUND AND ASSUMPTIONS

5.1 Waterborne sound

The waterborne noise is measured in terms of sound pressure, p. The sound pressure levels are presented in decibels (dB) relative to a reference sound pressure of 1 µPa, that is:

$$L_p = 10 \cdot \log_{10}\left(p_{\mathrm{rms}}^2 / p_{\mathrm{ref}}^2\right) \text{ dB}$$

Where:

$$L_p - sound\ pressure\ level$$
$$p_{rms} - root\ mean\ square\ sound\ pressure\ level$$
$$p_{ref} - reference\ sound\ pressure (1 * 10^{-6}\ Pa)$$

The results are presented in 1/3 octave frequency bands. Narrowband levels of the sound pressure levels are also presented with a width of 0.2 Hz.

5.1.1 Apparent underwater radiated noise

Ship radiated underwater noise is usually assessed and considered on the form of underwater radiated noise, i.e., a distance adjusted noise level measured by a hydrophone at a distance to the ship while passing. Alternatively, the noise level is adjusted for the Lloyd mirror in addition to the distance compensation, which is defined as source level.

When measuring underwater noise closer to the source, the recorded noise is not subject to the Lloyd mirror effect. The DNV class guideline for measurements of noise, DNV-CG-0313, includes a correction factor that enables the comparison of measured noise levels in the near field with criteria for underwater noise as measured by hydrophones in the far field. The correction includes both the Lloyd mirror effect and the correction for the solid boundary effect as the pressure sensors are mounted flush with the hull of -6 dB, and is presented graphically in Figure 5-1. The correction for Lloyd mirror assumes a source depth of 5 meters and a nominal far field distance of 100 meters. To summarize, the corrections applied to the measured levels to calculate the apparent underwater radiated noise levels are:

$$L_{RN} = L_p + 20log\, r/r_{1m} - C_r - 6dB$$

Where:

L_p = sound pressure level measured by pressure measurement device

C_r = Lloyd mirror conversion factor from source level as measured by pressure measurement devices to resulting radiated noise level as defined below:

$$C_r = 29\ dB - 16log(f), \quad f \leq 100\ Hz$$

$$C_r = -3\ dB, \quad f > 100\ Hz$$

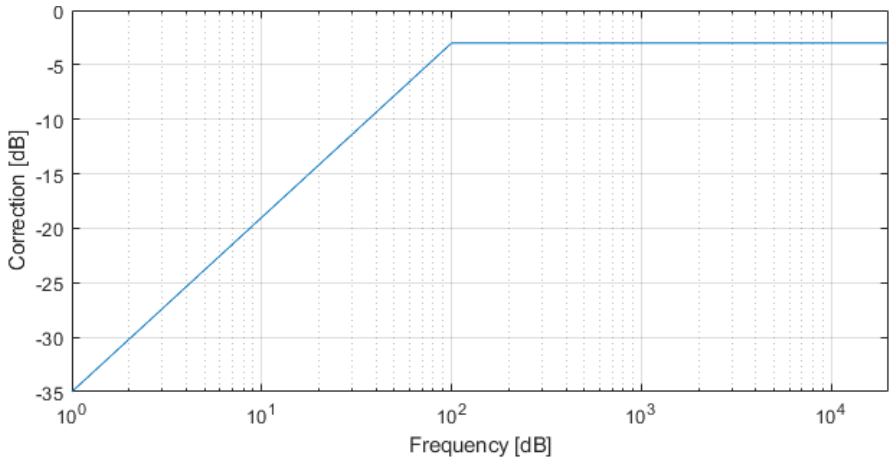

Figure 5-1 - Correction factor to estimate far field URN levels from near field pressure sensor measurements.

5.2 Vibration / Structure-borne noise

Structureborne noise is vibration, v, in the audible frequency range, which will generate noise when a vibrating surface excites the surrounding medium. The structureborne noise is usually assessed in velocity levels but may also be defined as acceleration levels. The measured levels are presented in linear levels in this report, but may also be presented in decibels according to the following definitions.

$$L_v = 10\log_{10}\left(v_{\mathrm{rms}}^2/v_{\mathrm{ref}}^2\right)\ \mathrm{dB}$$

Where:

$$L_v - velocity\ level$$
$$v - root\ mean\ square\ velocity$$
$$v_{ref} - reference\ velocity\ (5 * 10^{-8}\ m/s)$$

5.3 Airborne sound

The sound pressure levels are presented in decibel levels relative to a reference sound pressure of 20 µPa:

$$L_p = 10\log_{10}\left(p_{\mathrm{rms}}^2/p_{\mathrm{ref}}^2\right)$$

Where:

$$L_p - sound\ pressure\ level$$
$$p - measured\ rms\ sound\ pressure$$
$$p_{ref} - reference\ sound\ pressure\ (20\ \mu Pa)$$

6 INSTRUMENTATION AND EQUIPMENT

6.1 General

All instruments were installed at the same time, prior to all the work on the data processing. This means that everything had to be defined before knowing what the data looks like. Moreover, since the system was installed for a considerable amount of time, the installation had to be made at a detail level acceptable to owner and authorities as a fixed installation from a structural/fire integrity and safety point of view. The primary recording units are 2 located inside the pods and one main unit located in the propulsion room in the aft ship. From here, there is a cabled connection to the engine control room where it is finally stored.

Table 6-1 - Measurement equipment.

Location	Equipment	Make	Type
CL aft peak tank	Microphone	PCB	130E20
SB aft peak tank	Microphone	PCB	130E20
CL pod	Accelerometer, triaxial	Hansford	HS-173
SB pod	Accelerometer, triaxial	Hansford	HS-173
CL pod	Pressure sensor	Kistler	601CA
SB pod	Pressure sensor	Kistler	601CA
Propulsion room	Acquisition system (master unit)	IMC	Cronosflex
CL pod	Acquisition system	IMC	C-Series
SB pod	Acquisition system	IMC	C-Series
ECR	Measurement computer	Dell	Lattitude 5540

6.2 Pressure sensors

The ship in question is equipped with three propellers, driven by electrical motors mounted in pods. These are from now on denoted as two “wing” propellers and a “center” propeller in this report. As the two wings are symmetric during regular operation straight ahead, only one of the two wings is instrumented with a pressure sensor, in addition to the center propeller, to limit the number of hull penetrations. It was known from past experience that the acoustic modes induced by global vibrations of the pod strut due to torque fluctuations on the electric motor is dominating on the side of the strut. These modes have a very poor radiation efficiency due to their ”dipole”-like behaviour. To avoid contamination of the “onboard” pressure measurements by non-essential pressure fluctuations, the sensors were placed in front of the pod strut, just above the propeller plane. The sensors are of ICP type, charged directly from the acquisition unit and are fitted to an M14x1.25 threaded hole in the insert shown in Figure 8-2. As also indicated in the introduction to the report, the main purpose of the pressure sensors is to primarily pick up cavitation noise from the propellers, since a much more sophisticated set-up would have to be in place to map the complex acoustic modes from vibrations of the Pod. This is explained more in detail in Chapter 10.5 on MURN (Magnetic Underwater Radiated Noise Estimator).

6.3 Microphones

An attempt to indirectly measure the contributions from electromagnetic noise has been made by including microphones in the aft peak tank as well as accelerometers (See section below), but this was not a part of the scope of the current project. By using microphones, one can obtain an integrated mean level over the hull surface since the receiving location will be on the other side of a baffle exposed to forced vibration from the wet side which in turn radiates into the

void. The baffle will however give a frequency dependent response to a unit force, and each structural element will have a different response as well. I.e., this is a fairly complex modelling exercise and no attempts have been made to correct for the radiation efficiency. These are all added for exploratory reasons, and to extend the amounts of available data.

6.4 Accelerometers

Triaxial accelerometers have been included in rigid positions inside the pod structure, to monitor the energy level causing the shell of the pod to vibrate. The position is indicated in Figure 6-1, while a photo of a typical installation is included in Figure 6-2. The purpose of the accelerometers is to indirectly monitor the excitation coming from the pods, and to use the measured velocity levels as validation material for computations of vibro-acoustic radiation excited by the electric motor.

Since no cables can be pulled down to the pods, these sensors are hooked up to a separate data acquisition unit inside the pods which are synchronized with a two-pole cable through the slip-ring. The connection between these data acquisition units and the main unit in the propulsion room are moreover made wirelessly through a WIFI bridge. The accelerometers are ICP charged piezoelectric sensors glued to the stator of the electric motor.

A method to determine the radiated magnetic sound using stator vibration measurements together with magnetic noise simulation model (Digital Twin) was developed during the project. The Digital Twin produces both vibration and sound power response. The simulated sound power is corrected by matching the measured and simulated vibration levels at the same location on the electric motor stator (MURN adaptation).

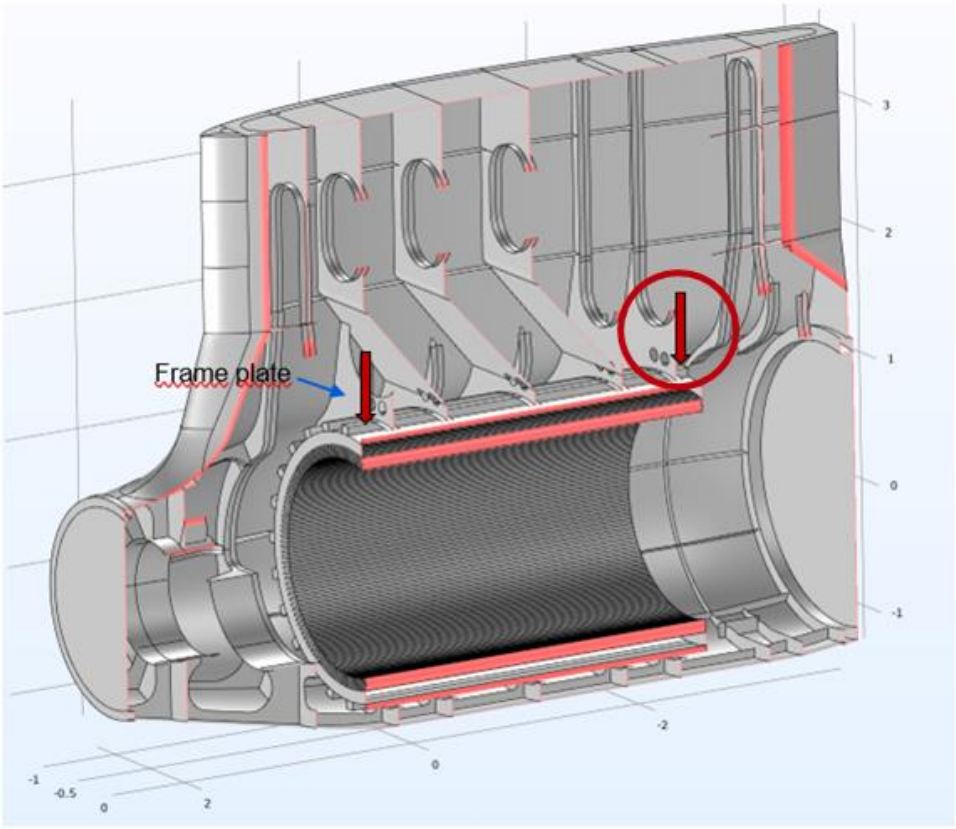

Figure 6-1 - Vibro-acoustical digital twin of a XO 2300 Azipod®. The location of stator vibration accelerometer is indicated by the red arrow inside the red circle

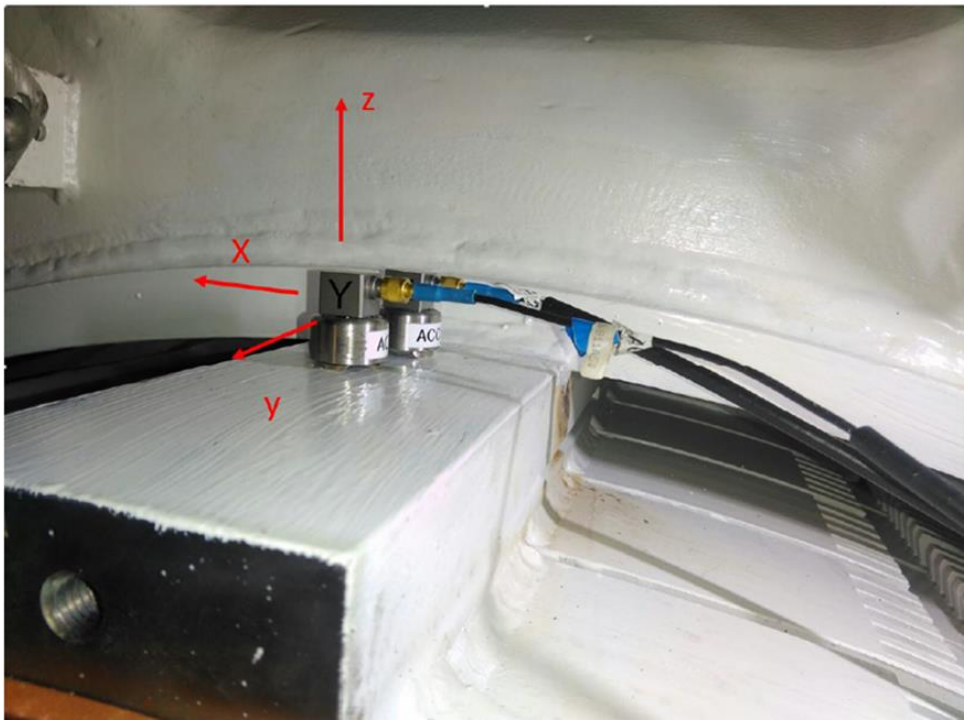

Figure 6-2 - Typical accelerometer attachment to stator yoke beam. The second sensor is for backup.

6.5 NMEA Data

National Marine Electronics Association (NMEA) has a standard format used by GPS transceivers to communicate information about position, time and movement. This data was used to obtain important data regarding the ships position and speed over ground.

As the NMEA data stream is continuous, serial connection to ship NMEA system via Serial Device Server in the ECR was used with the server itself connected to diagnostics network. The continuous NMEA data was further compiled in the RDS server PC into ASCII files each consisting of 1 minute flow duration and identified with time stamp. In this project the following NMEA data was used:

1. Vessel position ($GPGLL-NMEA keyword)
2. Vessel speed ($GPVBW -NMEA keyword)
3. Heading ($HEHDT -NMEA keyword)

6.6 CMX Data

CMX data refers to ABB Marine internal propulsion automation data format. During operation the propulsion automation system gathers time log data from various sources such as powerplant generators, propulsor frequency converters, ship navigation, etc. The number of quantities and parameters stored is vast and thus only a very minor data subsets were used in this project:

- Starboard pod
  - Shaft speed
  - Shaft power
  - Steering angle
- Centreline pod
  - Shaft speed
  - Shaft power
  - Steering angle

7 SYSTEM DESCRIPTION AND SETUP

7.1 DATA AQUISITION

In order to be able to continuously collect URN- and vibration data, modifications to the vessels diagnostic network are required. Additional measurement system instrumentation together with ship operational data collection framework were carried out. Figure 7-1 shows a high-level description of the system, Figure 7-2 gives an impression of the signal acquisition system additions and finally Figure 7-3 the network diagram of the CLUE-system.

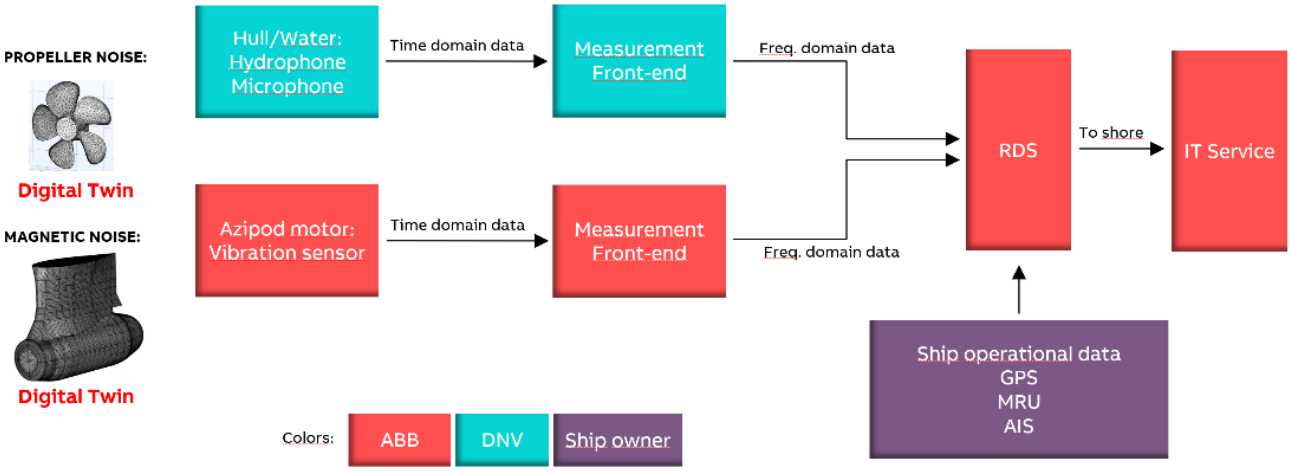

Figure 7-1 – High level block diagram of CLUE system.

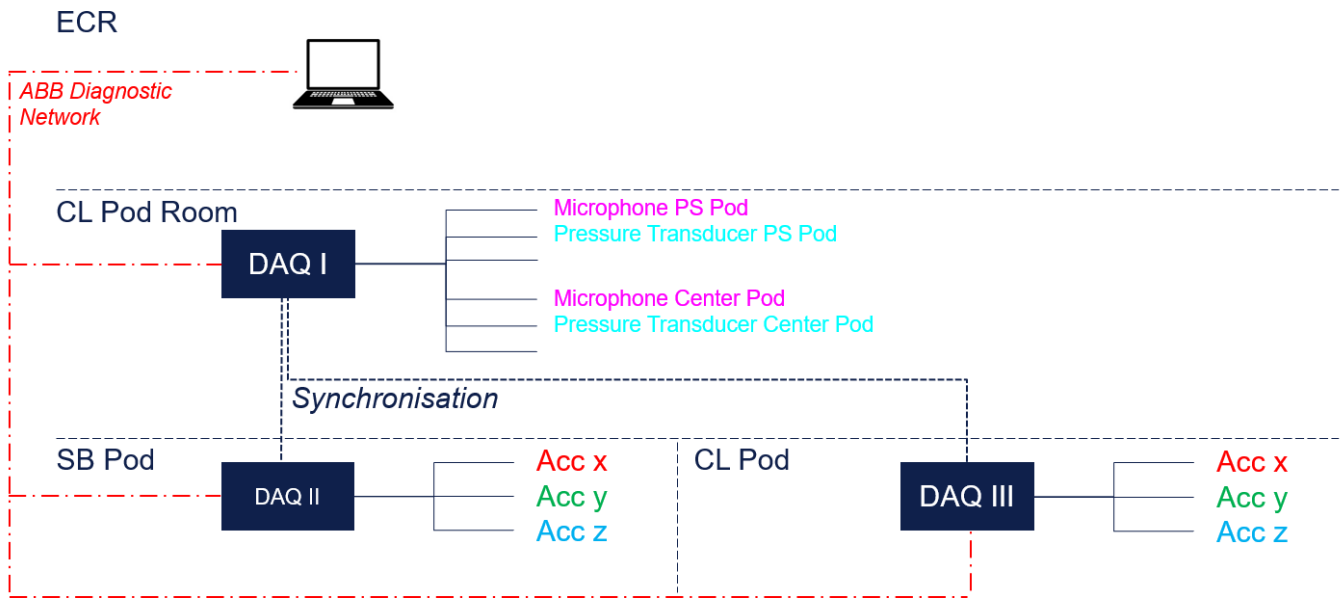

Figure 7-2 – The general concept of the measurement setup.

Each data acquisition task is explained shortly as:

1. Propeller noise: Microphone and Pressure Transducer installed in aft peak tank above CL and SB propellers connected to DAQ1 which is further connected to the diagnostics network.

2. Magnetic noise: Triaxial vibration sensors installed in CL and SB Azipod motor stators connected to respective DAQ units inside the Azipod. DAQs connected wirelessly to diagnostics network.
3. Azipod Propulsion Control data: Control network connected to ABB Remote Diagnostics System (RDS) Data Collector PC in CL converter room in separate physical interface. Data compiled and sent via diagnostics network to RDS server PC in the ECR.
4. Azipod Propulsion Drives data (CMX): Propulsion drives from respective Azipods are connected to data collector PC via separate network and physical interface. Data compiled in Data Collector PC and sent to RDS server in the ECR via the diagnostics network.
5. NMEA data: Serial connection to ship NMEA system via Serial Device Server in the ECR. Serial Device Server connected to diagnostics network and data compiled in the RDS server PC.

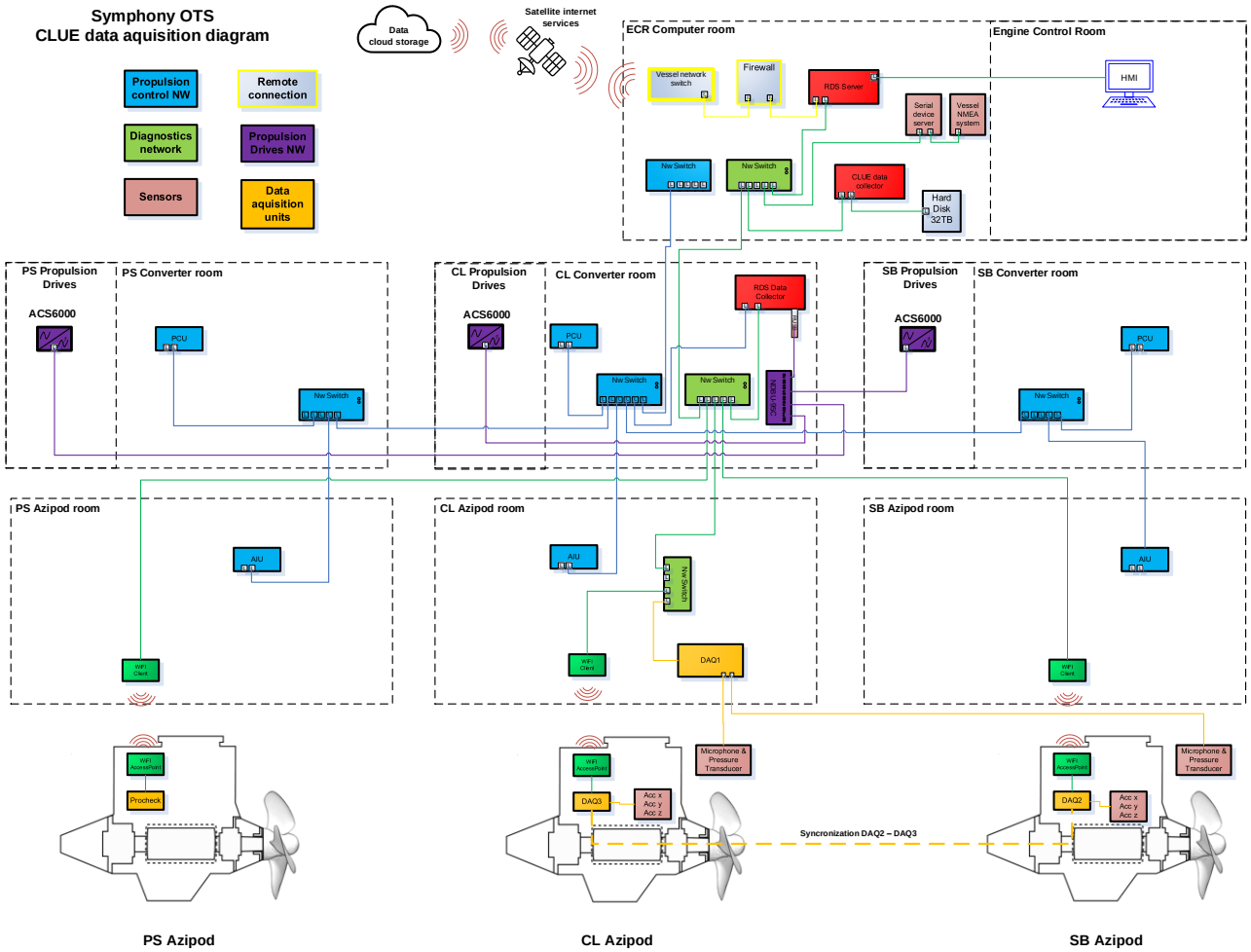

Figure 7-3 – Network diagram of the data acquisition system.

7.2 DATA TRANSFER

The acquired raw data was stored locally on a large hard-disk, since the amount of the data would have exceeded the remote connection capacity. Some processing took place in the system (time -> spectra), the results of which could be

transferred through the remote connection together with the CMX- and NMEA-data. The primary stage of the data transfer is the vessel's RDS computer as explained in below:

- Propeller and magnetic noise data: Data is being read on the CLUE data collector PC and raw data is being stored on external harddrive in the ECR capable of storing several months of data. Post-processed measurement data is being sent to RDS server PC in the form of 1/3 octave band spectra for the pressure sensors and microphones and narrowband spectra for the vibration measurements.
- Azipod Data (CMX): All Azipod operational data is being stored by the RDS system locally for up to one year.
- NMEA data: Read directly and stored to the RDS server PC for up to one year.
- All data related to CLUE project is gathered in the RDS server PC in the ECR. RDS server sends data to ABB cloud servers via the ship satellite internet which is connected to RDS server via dedicated hardware firewall.

7.3 CYBER SECURITY

As it is obvious with modern IT systems, one should always pay attention to data and system security while operating with data transfer. For completeness, the following list gives a short insight into the concepts and measured to ensure IT-safety of the system:

- ABB has possibility to remotely connect to RDS server via the remote connection to check system health and modify parameters. This is done via ABB Remote Access Platform (RAP).
- Hardware Firewall opened outbound to 2 predefined IPs over 443 (https)
- Encryption (TLS/SSL standards)
- Secure tunnel between ABB and Vessel RDS server
- All data is encrypted
- Communication is all outbound from Vessel to ABB
- All RAP users managed by strict permissions
- All support scenarios are reported and auditable at support provider and customer sites
- Remote access sessions all controlled by customer from the ECR RDS user interface

8 SYSTEM INSTALLATION

Installation of the system onboard the ship was carried out in March/April 2023 while the vessel was in drydock in Navantia Shipyard in Cadiz, Spain. The installation was carried out according to requirements for permanent installations. This necessitated additional efforts compared with the conventional opportunistic installation methodology.

More details on the different sensors that were installed can be found in Chapter 6.

8.1 Stainless steel inserts

Vital for the installation of the system was the installation of the pressure transducers. The pressure transducers are made of stainless steel. Regularly, the sensors can be installed directly through the ship hull by drilling a hole with the right dimensions and threading the hole to be able to insert the sensor correctly. This form of installation is usually done for a duration of days, up to a week or two. Direct contact between the stainless-steel pressure sensors and the carbon steel hull would most likely lead to excessive corrosion, damaging the sensors. This is one of the reasons for installing the sensors in inserts which again are welded to the shell plates.

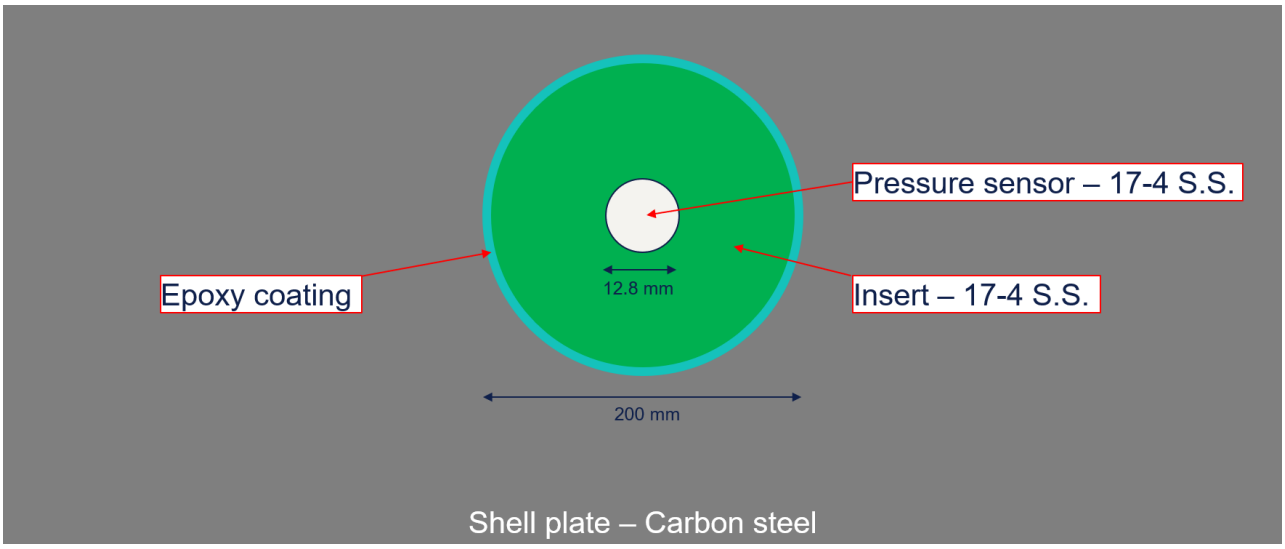

Figure 8-1 - Sketch of stainless steel insert in the hull.

Figure 8-2 - Insert for pressure sensor

9 ANALYSIS AND DATA PROCESSING

9.1 General

The data is stored in two separate formats on our cloud server. One file containing the CMX data files containing all the nautical data with timestamps according to UTC, and one set of files fully synchronized to sample level from the data acquisition unit(s). One of the issues that was encountered during the data handling was that the two files are not stamped with a common time stamp, since all clocks will drift to a certain level (except the one synched with UTC). To synchronize the two datasets, correlation was made on the rpm feedback from the operational data and the processed blade passing frequency from the pressure signals stored in the sensor data.

9.2 Source level heatmap

While the system has been installed, the vessel has mainly been operative in the Mediterranean Sea. It has been sailing between the ports of Spanish, French and Italian cities of Barcelona, Mallorca, Marseille, La Spezia, Rome, and Naples.

Through continuous measurements, vast amounts of data are gathered. This may be used by different stakeholders. For example, by using an overview of the sailing plan as presented in the figures below, there is potential for adjusting the planning of the itinerary to optimize for low-noise operation.

The figures show the rms pressure in 1/3 octave band from 100 Hz to 20 kHz. The measured levels have been adjusted according to the differences between the levels recorded by the pressure sensors and the hydrophone during the calibration measurements, i.e., a derived transfer function.

For comparison purposes, results from weeks 16 and 17 are included. The overall trend looks similar when comparing the two weeks. However, there are differences, e.g., when entering into port and the performance after passing through the strait between Corsica and Sardinia.

From the figures, it seems like the time between the ports requires the vessel to sail at similar power between most of the ports. While between e.g., Barcelona and Mallorca, where the distance is lower and after passing Corsica and Sardinia, the vessel has more time to reach its destination and is therefore able to reduce the speed and power. If combining source level heat maps with detailed maps over areas where sensitive species of marine life are based, this can also be optimized to reduce the influence of the ships in operation in these areas. The concept of the source level heatmap can also be expanded with more vessels equipped with similar systems. The potential will be vast for reducing the influence on sensitive species by using the gathered information effectively to optimize sailing patterns and tune regulations to be as efficient as possible.

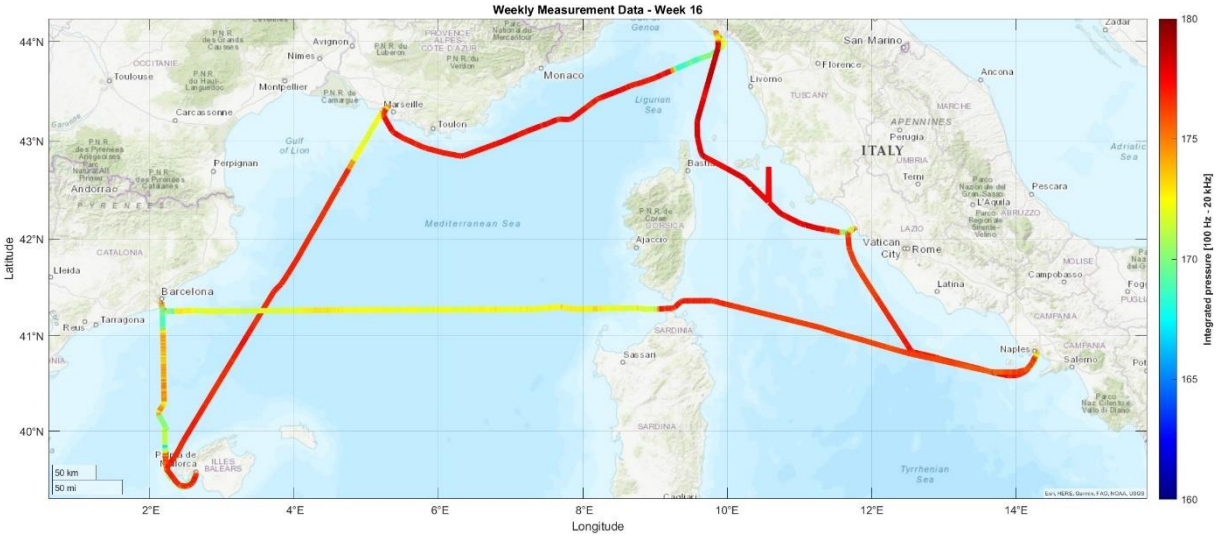

Figure 9-1 - Source level heat map week 16.

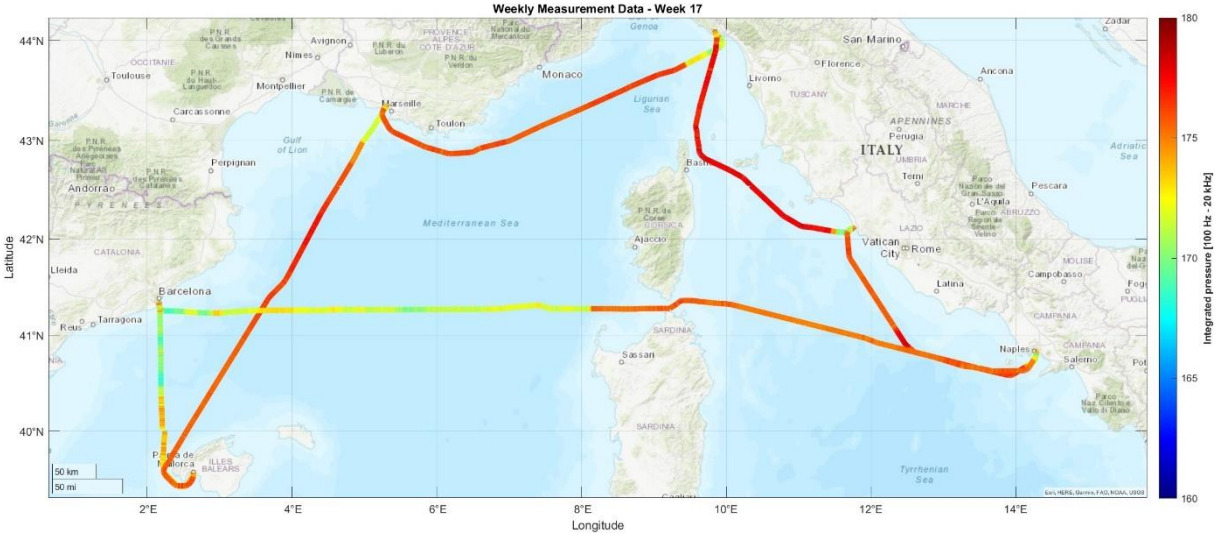

Figure 9-2 - Source level heat map week 17.

9.3 Overview of recorded data during a one-week voyage

A large amount of data is constantly being collected. It was chosen to demonstrate some of the possibilities concerning data processing with high time resolution on a finite data set. The data selected for the demonstration is from May 1st to May 7th. In Figure 9-1. To condense the operational data to be suitable for visualization purposes, the plot given in Figure 9-3 was prepared.

The top figure shows the propulsion power, the middle shows the rpm/speed and the bottom shows the angle for the centre pod. The coloring of the plots (red and blue) indicates whether or not the levels from the hull pressure exceed a certain level. Red is below the threshold and blue is above. It is clear from the plots that increase in power increases the likelihood of exceeding the criteria as expected. It is also clear that the levels stay high for a larger speed range during a deceleration compared to an acceleration. Possible causes of this behaviour are discussed later.

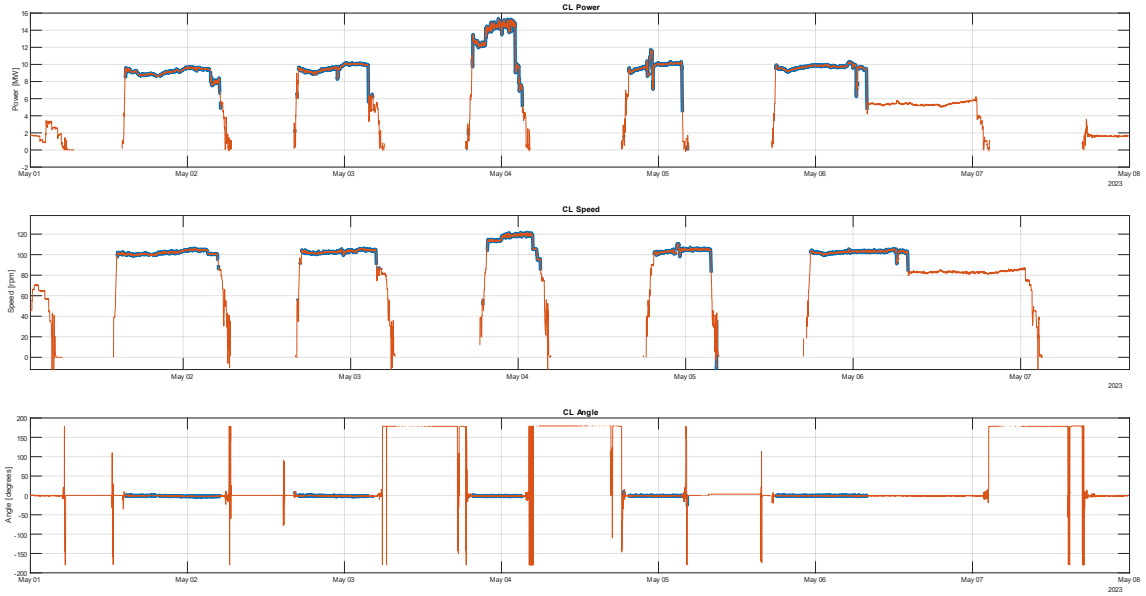

Figure 9-3:CMX data from week 17

9.4 Special events

The overview plots like the one in Figure 9-3 were used to pick out interesting events for further analysis with higher resolution and more information, for instance like the spectrogram presented in Figure 9-5. Unlike Figure 9-3 where the data values were simply based on a Boolean, e.g., if one frequency band is above the limit or not, Figure 9-5 shows a significantly smaller time period but with a full frequency analysis of the recorded sound pressure level during the run up from 14:00-15:00 on May 1st for the centre pod. Please note that this particular plot is not corrected for solid boundary factor or any other propagation effects. It can however be used to identify what frequency bands are dominating, and how dominating they are. By knowing the dominating frequencies as well as the behaviour as a function of time, taking into account the drive parameters from zooming in on Figure 9-3, one can better understand the underlying physical mechanism causing the exceedance. By using this information to narrow down your number of suspects, one may be able to apply corrective measures to target this/these mechanism(s). A particular effort was made to analyze the areas where the behaviour of the pressure signal resulted in a transition from being just above to just below the given criteria. As stated above, it is evident from Figure 9-3 that the propulsion power is strongly correlated with noise levels above the criteria. This is also supported by other ongoing work and is possibly the most trivial cause, at least if it is due to the influence of increased power on tip vortex cavitation or other cavitation types.

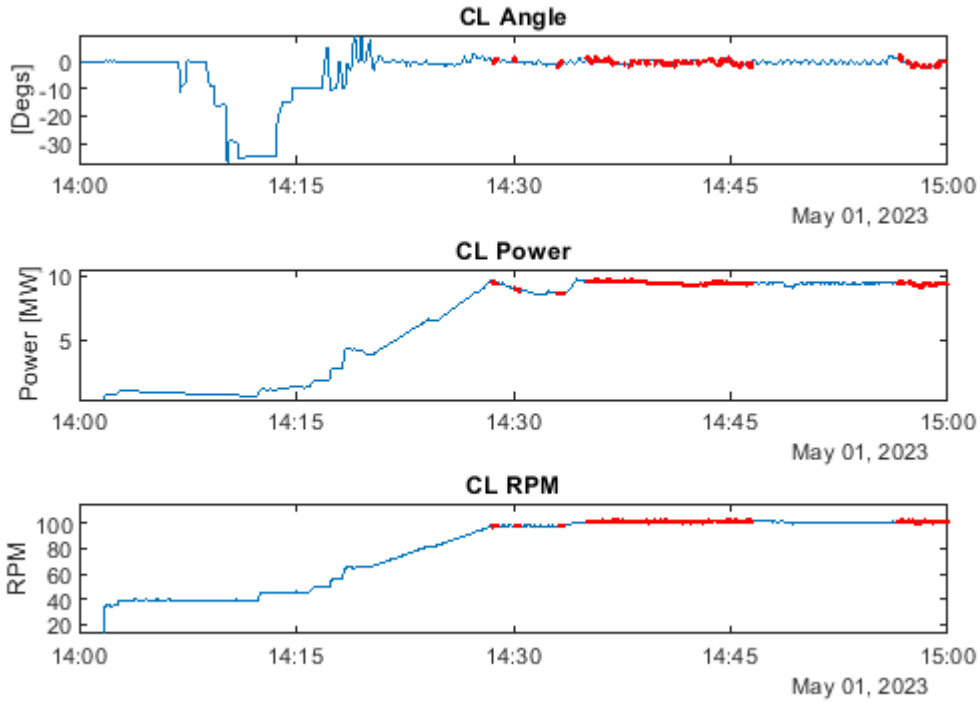

Figure 9-4 CMX Data with a zoomed in overview plot

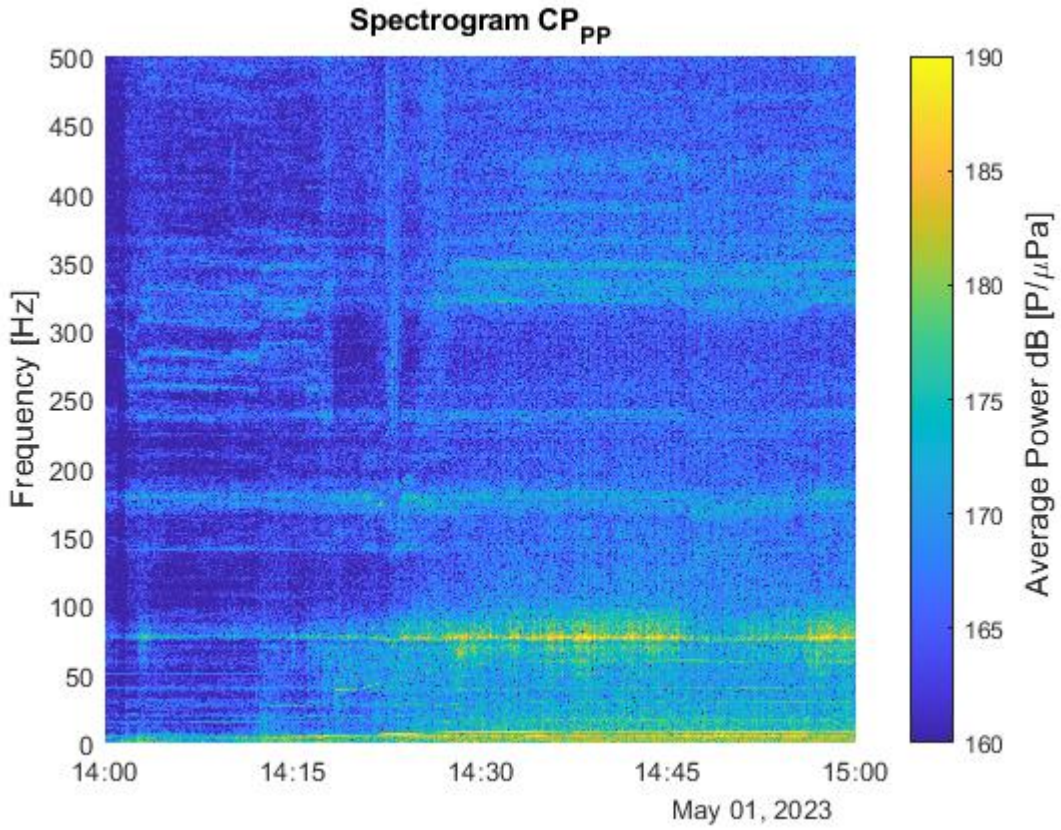

Figure 9-5: Spectrogram Centre Pod Pressure Pulses

Unlike what one would expect, considering the strong correlation between the recorded sound pressure level and the power, there is a distinct fundamental frequency around 80 Hz including higher harmonics. This phenomenon is expected and is likely caused by weak singing of a component located close to the location of the pressure sensor. Singing is a rather common phenomenon, where vortex shedding, typically at the trailing edge of a structural element immersed in water, coincides with one of the fundamental natural frequencies of the structure. During a run up, the shedding frequency will first increase linear to the speed until the shedding frequency coincides with the natural frequency. From that point, the shedding frequency locks in with the natural frequency so the structural natural frequency starts to govern the frequency of the shedding process. The lock-in span can be quite large depending on the complexity of the vibration mode excited. The same will occur if it is possible to start at a speed higher than the upper limit of the lock-in span and run down in ship speed. The vortex shedding locks in with the structural natural frequency at some point and stays locked in until it goes below the minimum speed of the lock-in span. It is difficult to see the increasing frequency as it is dominated by random excitation of the same mode either through mechanical vibrations or random pressure fluctuations in the water column. If one measured closer to the singing element, it is believed that a clearer trend would be seen. This is a known phenomenon, and for reasons to be explained, it is not of particular concern with respect to far field URN. The singing has been encountered before and is created by a vibrating plate which is very easily excited. Since the fundamental mode of the plate has a trivial simple mode shape that can be modelled through a distribution of monopoles with opposite signs on each side of the plate, the pressure on a distance of the order of the length scale of the separation of the sources will be a dipole. On a much larger length scale these sources cancel out and results in a very poor radiation efficiency.

Another set of frequencies which are also distinguishable is the blade passing frequency and its harmonics, in the range of about 10 Hz, the magnitude of the components can be seen to be governed by the propulsion power. These components are however from non-cavitating effects with limited band width. The first harmonic is normally seen as a poor radiator, as it is due to the displacement of the blade and can therefore be considered a dipole-like phenomenon

with dipole moment according to the chord length of the blades. If sheet cavitation occurs at higher loading, it becomes a more efficient radiator since the phase transition will result in a mass source of monopole-like nature which is an efficient radiator.

In Figure 9-4, the CMX (operational) data is presented for the same time interval, i.e., it is the same data as Figure 9-3 but it is focused on the same time interval as the spectrogram. In oppose to Figure 9-3, the red line indicates the moments where the pressure fluctuations exceed the requirements and shows for obvious reasons good correspondence with the overview plots in Figure 9-3. When reaching a power of about 10 MW the tonal noise at 80 Hz exceeds the defined limit. To ensure that it is indeed the 80 Hz frequency that is the main reason for the exceedance, 1/3-octave band frequency spectra were calculated every second and presented in the same graph in Figure 9-6-.

The levels in Figure 9-6- and Figure 9-7 are plotted as apparent URN sound pressure levels at 1 m distance , meaning that they are corrected for distance, boundary reflection and Lloyd mirror to be comparable with regular RNL levels for underwater noise. The distance correction is assuming a monopole in free field, i.e., spherical spreading. As seen in Figure 9-6-, as previously stated, the 80 Hz is indeed the main factor of exceedance. As it will be shown later on through measurements that the argument from above concerning the radiation efficiency is valid, these components can normally be filtered out in order to get a better insight into the parts of the source which are influencing the far field URN.

As seen in Figure 9-6, the measured noise levels are relatively high for lower frequencies. As the contributions to the noise levels at 80 Hz are known, and considered to be less relevant in the far field, attempts were made filter out these components. To find strong contributions in the noise spectrum, a filtered spectrum can be more easily used as it is not as perturbed by the 80 Hz phenomenon. From 23:00 to 00:00, between 3rd and 4th of May, the power is between 14 and 15 MW. This is the interval with the highest average power during the current week. To further investigate the corresponding frequency content in this time period, a series of 1/3 octave band spectra with 1 minutes of window length, are plotted in Figure 9-7.

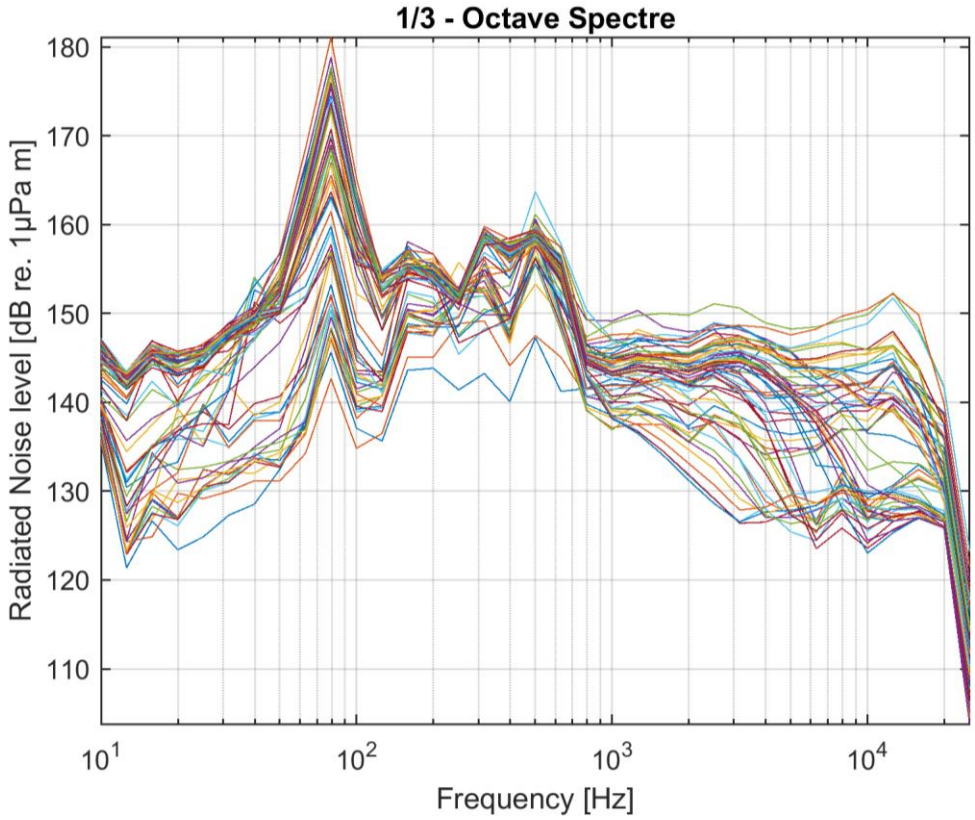

Figure 9-6- 1/3 – Octave band spectra presented as "apparent" URN levels, 14:00-15:00 on 1st of May 2023

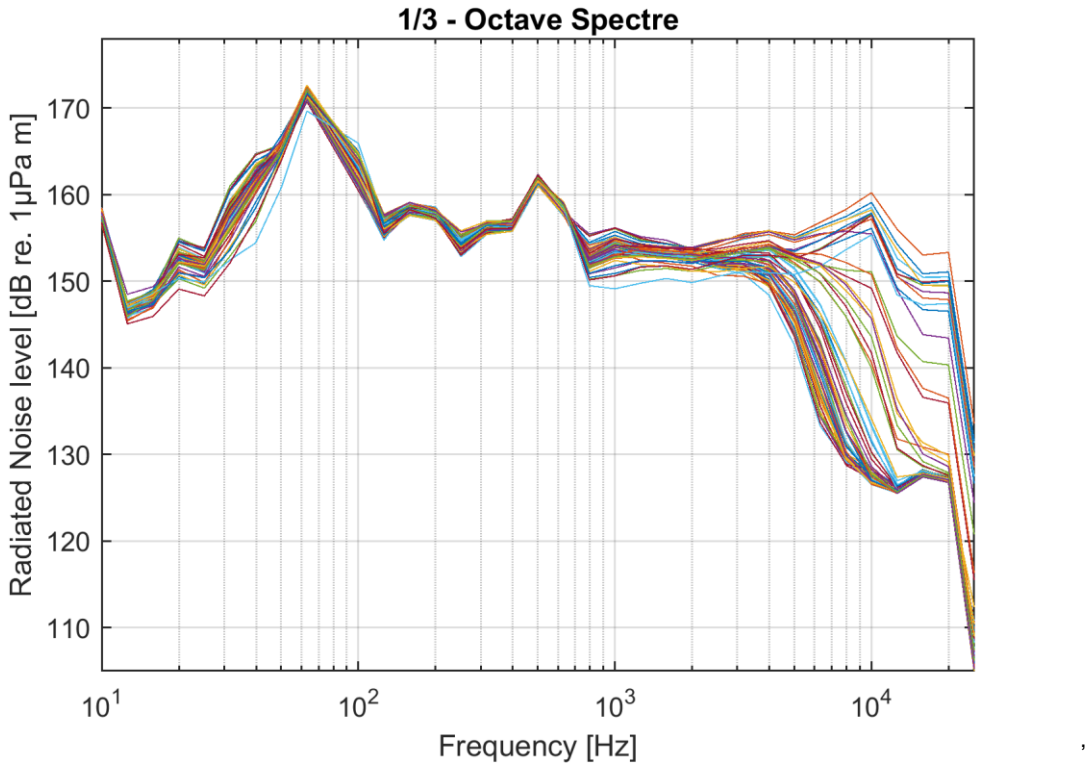

Figure 9-7 Octave Spectra apparent URN, 1 min windows for 1 hr between 23:00-00:00 on 3rd to 4th of May 2023

Figure 9-7 shows that the low frequency domain still has a considerable energy content associated with it, despite the attempt to filter out the frequency band containing 80 Hz. There is however also a significant contribution from around 10 kHz which is non-stationary and exceeding the median spectrum by 10-20 dB. A spectrogram with high frequency resolution is plotted in Figure 9-8 to further analyse the cause of this behaviour. The figure shows a quick increase of pressure levels for short time periods for a large frequency range above 750 Hz, which is not constant nor periodic. To identify what may be causing this phenomenon, the CMX data for this time interval is displayed in Figure 9-9. Here, the window length is lowered to a length of 1 second, to enable identification of possible rapid fluctuations in pressure levels. To further elaborate on the possible causes of these fluctuations, the actual time series is presented in Figure 9-10.

There is no obvious correlation between the CMX data and the elevation of higher frequency components. There could be signs of a correlation between higher power at around 15.5 MW together with increased RPM fluctuations. The correlation is however extremely vague and is currently not resolved. However, it is clear from the time series shown in Figure 9-10 that the pressure amplitude is indeed higher and more intermittent when the exceedance occurs and that it is not caused by the singing phenomenon at 80 Hz. Considering the large number of windows where these higher frequency components are not present, both from Figure 9-7 and Figure 9-6-, one can consider finding these components as an advantage of continuous monitoring of pressure signals. If recordings were made over the normal time interval, as presented in the calibration measurements in chapter 10, one would most likely not have found this trend.

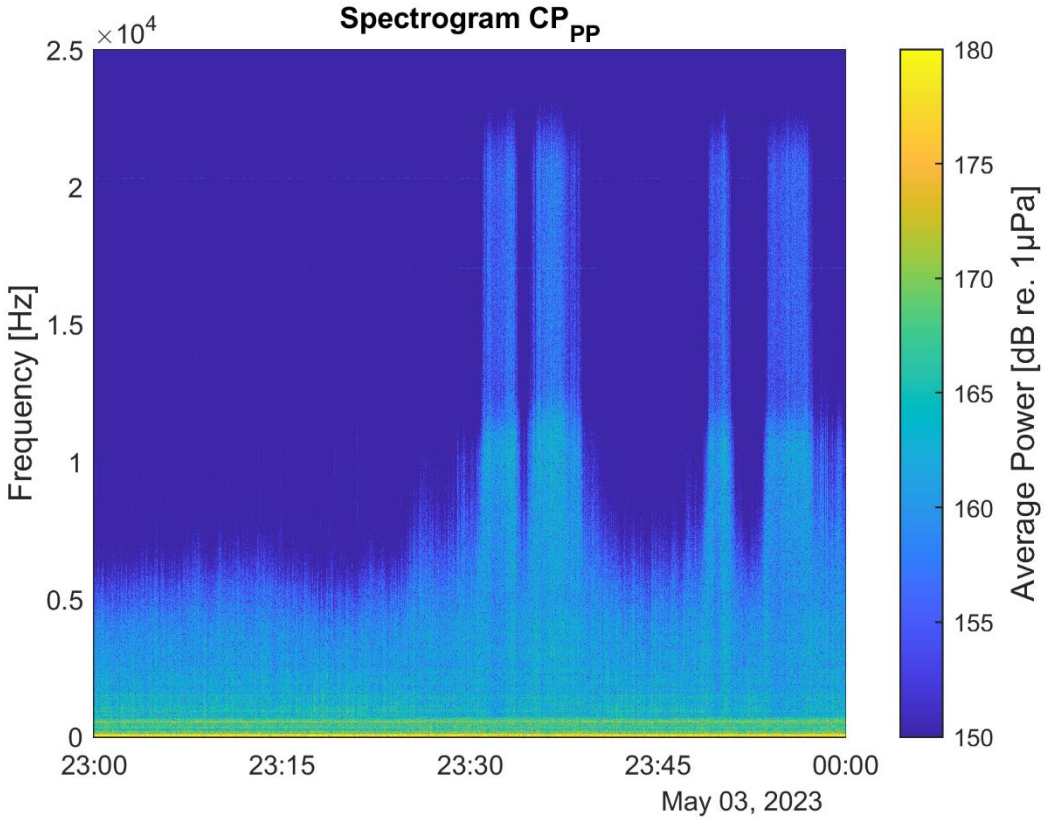

Figure 9-8:spectrogram showing the narrow band representation of Figure 9-7

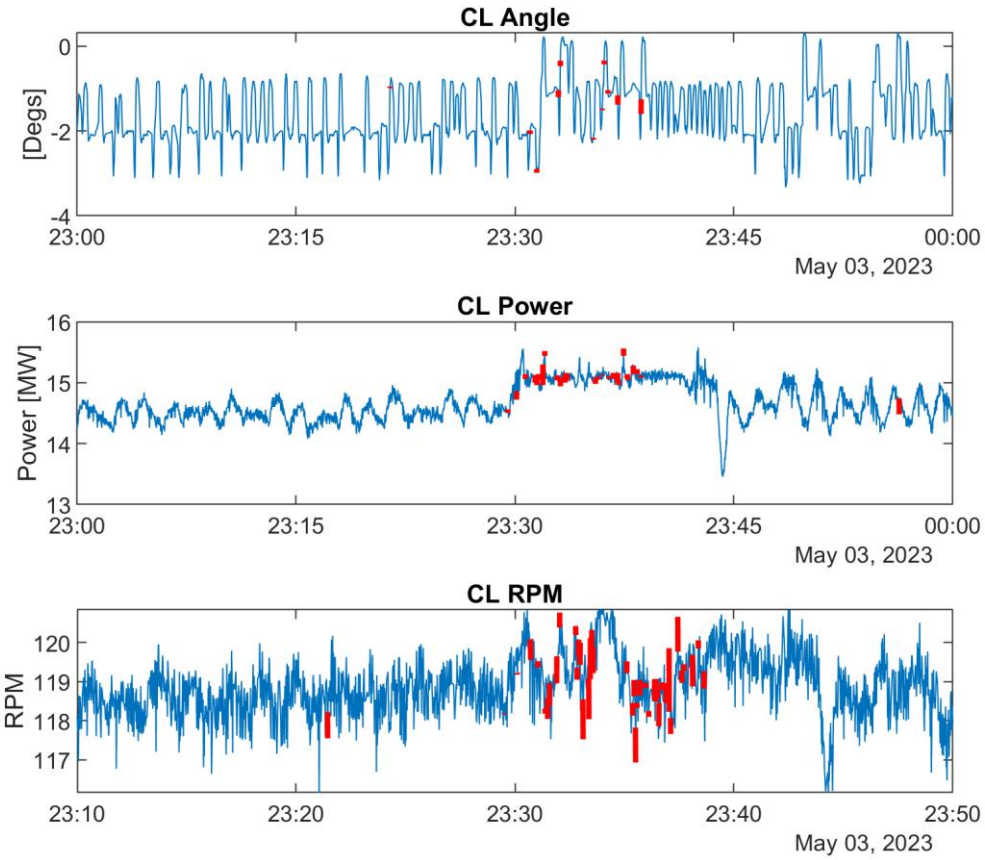

Figure 9-9:CMX data for the time interval presented in Figure 9-8

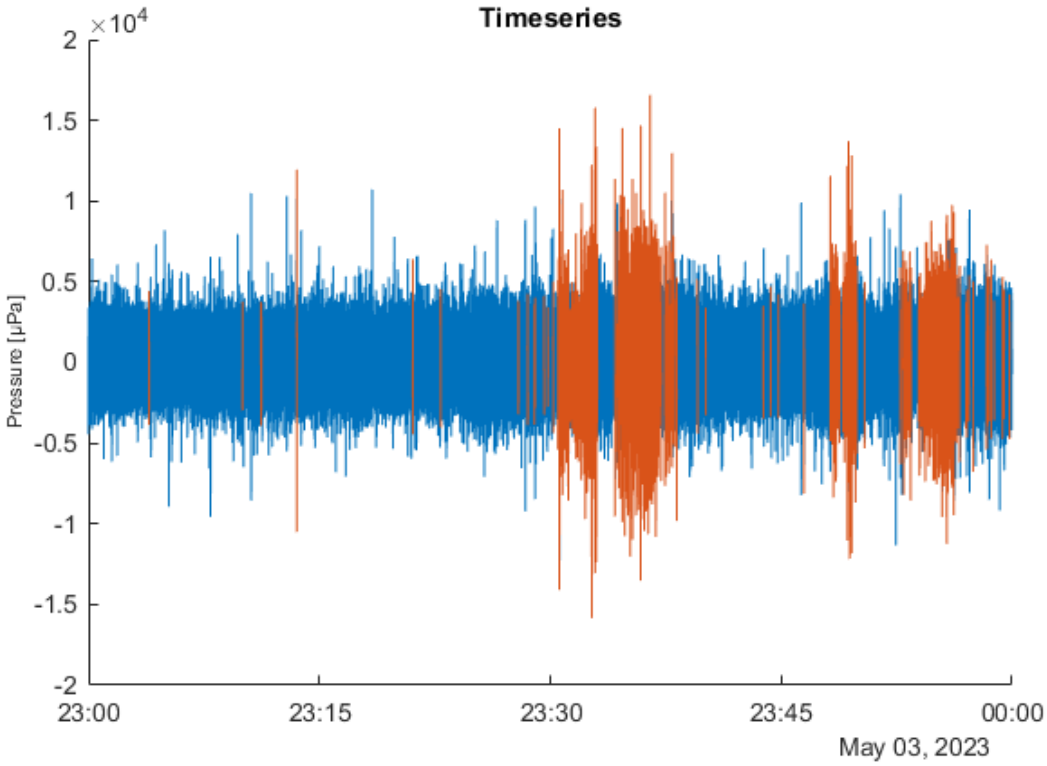

Figure 9-10:Time series showing a linear representation of the pressure fluctuations

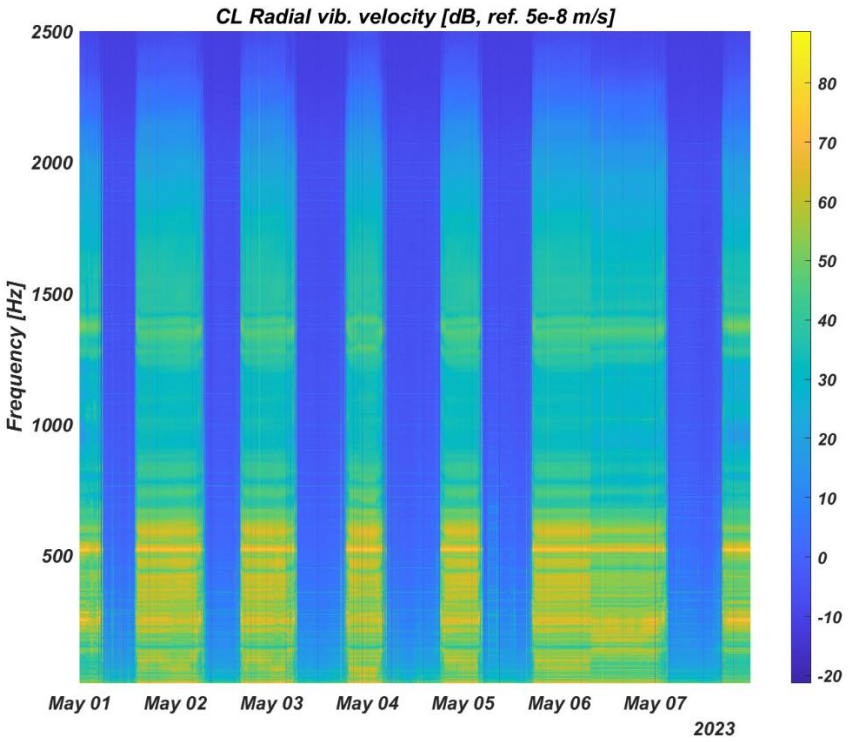

Figure 9-11: Spectrogram Centre Pod Radial stator vibration

Another finding, which is quite apparent from all presented plots is a common peak for all the presented frequency plots around 500 Hz (520 Hz). The frequency is seemingly independent of ship speed and there is no clear correlation between power and amplitude. For reasons to be explained in further detail in a following chapter, it is believed that this part can be augmented through computations to enhance the correlation between near and far field measurements. For now, it will just be pointed out that the pressure is generated by excitation of a fundamental vibration mode of the stator through electromagnetic excitation, hence it is often referred to as “magnetic noise”. A spectrogram illustrating the vibration response of the stator in the radial direction, is given in Figure 9-11 for the week subject to analysis in this chapter. There is a constant frequency component at 520 Hz always dominating this part of the frequency range, although the speed and power has been varying according to the CMX data presented in Figure 9-3. In \hapter 10, this component is discussed more in detail, both with regards to cause and the implications it has on the far field radiated noise.

9.5 Propeller induced broadband excitation.

All the components discussed for now, with the exception possibly of the blade rate harmonics are complex phenomena from a near field sampling perspective. The primary source of noise from ships, however, stems from propeller cavitation. Propellers produce cavitation at certation rotations per minute. The pressure difference from the angle of attack and the fluid velocity past the blade section casus cavitation primarily on the suction side of the blade. When the bubbles from the cavitation collapse it releases broadband noise. Two main types of cavitation is induced from the propeller, tip vortex cavitation and sheet cavitation. For the broadband noise, it is mainly the tip vortex cavitation who produces the broadband noise. Tip vortex cavitation is on a general basis due to the phase transition from water to vapour inside the core of a lift generated vortex coming from the tip of the propeller. More detailed, the radiation of noise primarily comes from oscillations of the interface between the phases, the changes in production rate of vapour and due to collapse of the vortices. A small contribution to broadband excitation also comes from small variations in harmonic content of sheet cavitation and bubble, but this is expected to be of limited importance because sheet cavitation is not significantly present for the current propellers except for at higher loading The bandwidth of this contribution is limited.

A key objective of this project is to implement a cavitation detection system. At first, it was believed that an instantaneous evaluation of pressure at all times would be able to provide information regarding whether or not the propellers were cavitating. Theoretical evaluations, as well as experience shows that an increased power associated with stronger tip vortices elevates the high frequency range. At low power output where the propeller drops below the inception point, the higher frequencies drop. It is believed that at some power, when the tip vortices go below cavitation inception, the slope of the higher frequencies as a function of power will change.

Defining a dB threshold for an average power over a bandwidth was deemed a possible solution. In Figure 9-12, one minute blocks of data are processed and presented for an entire week as a function of power. As can be seen there is a clear trend that the noise increases nearly linear with power at the upper frequency range from 1-10 kHz, from around 4 MW and up to 14. However, between 2-4 MW the slope seems to be significantly stronger. This area is also from the dataset among the areas where there is a substantial variation in the measured amplitude. It is believed that this noise will confuse a cavitation detection system which is working with instantaneous measurement data. However, it is suggested after analyzing the data, that a system based on long term statistics seems to be significantly more realistic. The system could of course be updated on a weekly basis based on the statistics of the previous week to account for performance differences due to fouling and other factors. Figure 9-8 also suggests that there is a high degree of variability in instantaneous spectral content although the average shows comprehensible trends. The suggested detection system for the dataset in Figure 9-8 would give the output “no cavitation” below 2 MW and “cavitation” above.

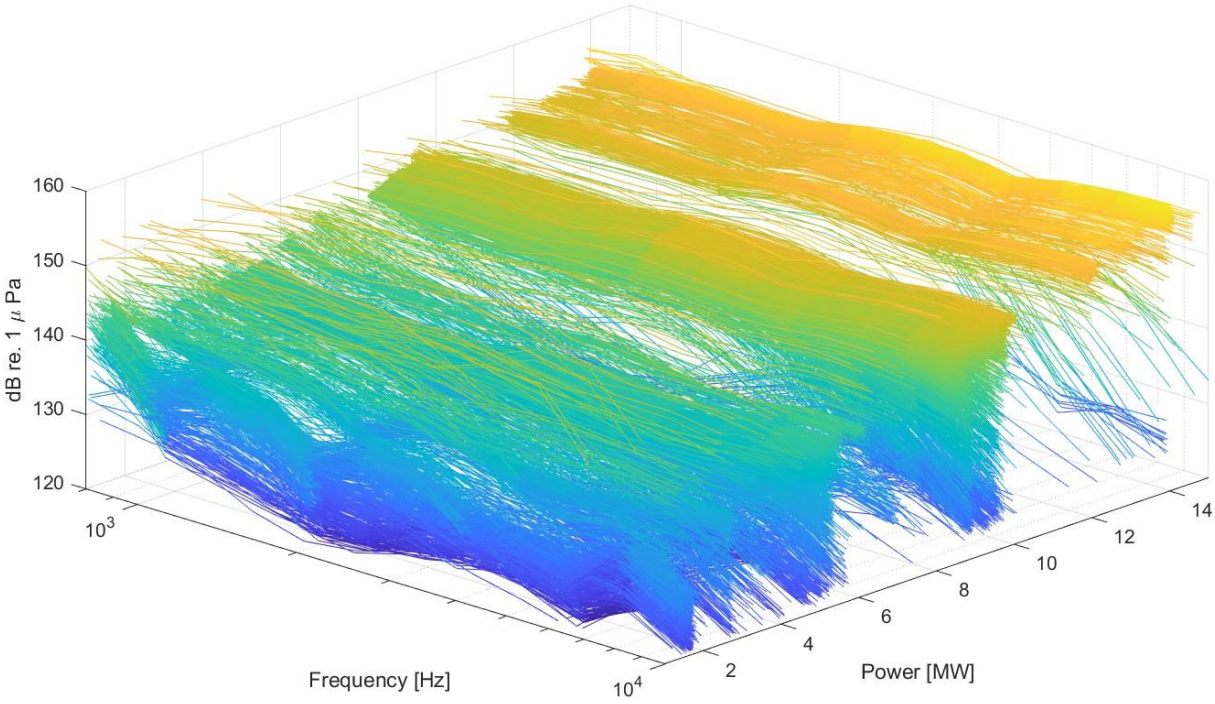

Figure 9-12 - CL pod noise level spectra vs. CL power for frequencies between 800 Hz and 10 kHz.

10 CALIBRATION MEASUREMENTS

10.1 General

The idea behind the methodology presented in this report, is that there is a simple relation between the pressure emitted in the near field by the most dominating sources, and the far field underwater radiated noise from the ship. Of course, to utilize the methodology with only one sensor and no other available information, one must apply a number of assumptions. In this work, it is assumed that the transfer function is only depending on the distance and frequency, and that all sources transferred from near to far field are located in the same point on the hull. This is only true if each frequency component is dominated by the same acoustic mode shape for each ship speed/power setting. As argued for in chapter 9, this is not entirely true if the pressure signal is used directly without knowing the applicable frequency ranges, as the pressure signal is contaminated by other factors. Previous experience has however shown that this is a good approximation for propeller induced noise, which is expected to be one of the most dominating factors to far field URN. It is important to keep in mind that the frequency content due to electromagnetic excitation and radiation from the pod structure will be augmented by a digital twin/vibroacoustic computations supplied by ABB.

For calibration and correlating the measurements carried out with sensors onboard, with measurements of underwater radiated noise a trial was carried out while the ship was in service. The far field underwater radiated noise measurements were carried out with hydrophones in the water column outside Mallorca/Spain in June 2023 during normal operation of the vessel. The operator was cooperating by changing the vessel's trajectory somewhat to facilitate the measurements for CLUE. As the vessel was sailing with passengers onboard, the measurements were limited to two passages of the hydrophone setup; one passage south-bound on the voyage between Barcelona and Palma and one passage north-bound between Palma and Marseilles.

The operating conditions used for calibration were chosen to be close to or at the operating conditions referred to in the DNV Silent notation, for reference. However, it should be noted that what is termed the 80% operating condition is conducted at a somewhat lower power.

10.2 Equipment and setup

Three hydrophones, two iClisten RB9 type and a Reson TC4032 hydrophone were deployed. More details about the hydrophones are presented in Table 10-1.

The iClisten hydrophones are so-called autonomous hydrophones where the measurements are stored internally as .wav files, while the Reson hydrophone is used together with a noise level meter of Norsonic Nor140 make for recording and live monitoring of the measurements. I.e the latter hydrophone is connected to the handheld measurement equipment by cables, which in turn is physically monitored through a headset while recoding to ensure good data quality.

Table 10-1 – Description of hydrophones

Hydrophone model	Serial number	Sensitivity @ 250 Hz [dB re. V / µPa]
iClisten RB9-ETH	6139	-176.6
iClisten RB9-ETH	6467	-177.2
Reson 4032	3310070	-167.2

The hydrophones were deployed at depths and distance to closest point of approach (CPA), i.e the minimum distance between the hydrophone and the ship, as described in Table 10-2.

Due to unforeseen issues experienced during the tests, the hydrophone setup was altered between the two ship passages. At 80%, two hydrophones were located at the seabed and one was hanging in the water column about 15 meters below the sea surface. However, at 11 kn only the two bottom mounted hydrophones were reported.

Table 10-2 - Depths and CPA distances of the hydrophones.

Hydrophone model	Serial number	Depth [m]		CPA distance [m]	
		11 knots	80% MCR	11 knots	80% MCR
iClisten RB9-ETH	6139	79	18	123	120
iClisten RB9-ETH	6467	79	79	123	120
Reson 4032	3310070	79	79	120	100

Figure 10-1 and Figure 10-2 shows the measurement setup and geometry, while Figure 10-3 indicates the vessel sailing path during the measurements as well as the hydrophone deployment locations.

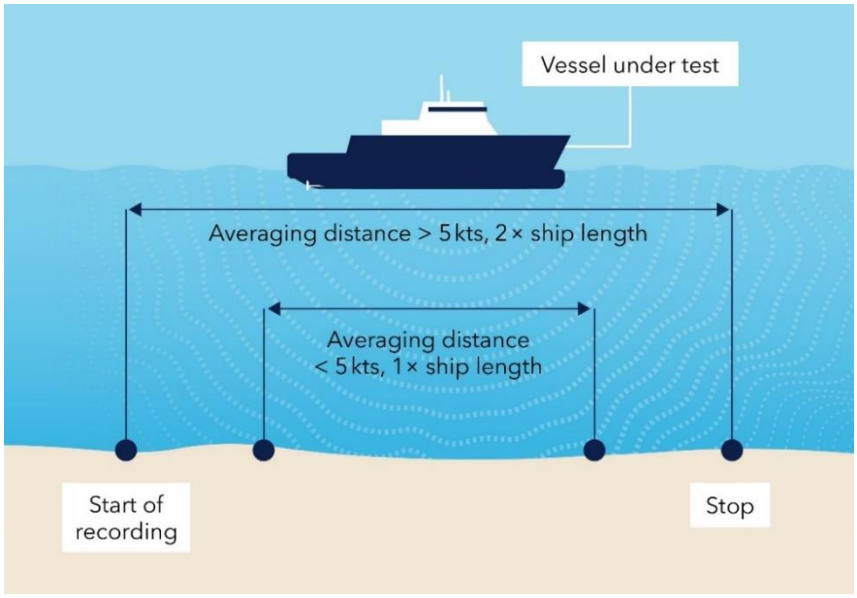

Figure 10-1 - Sketch of time window.

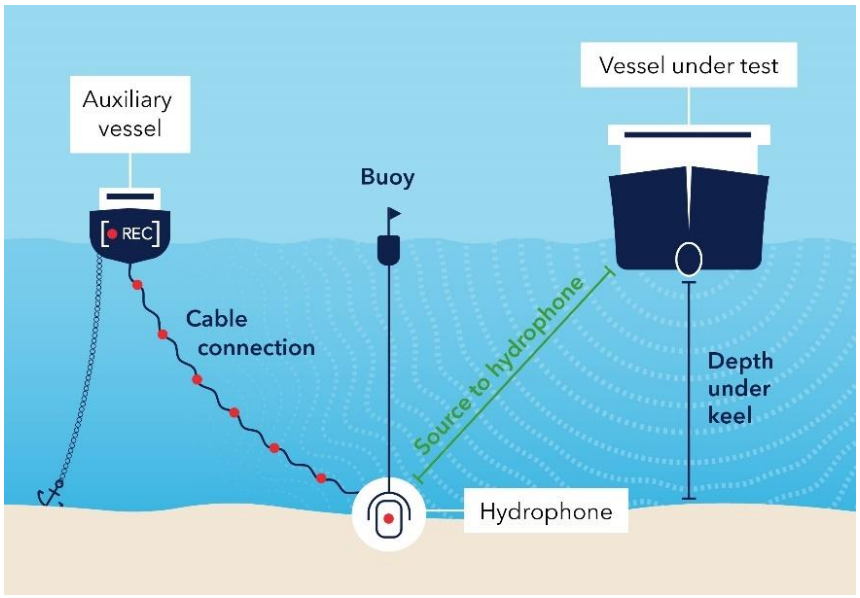

Figure 10-2 - Sketch of measurement geometry of a single bottom-mounted hydrophone.

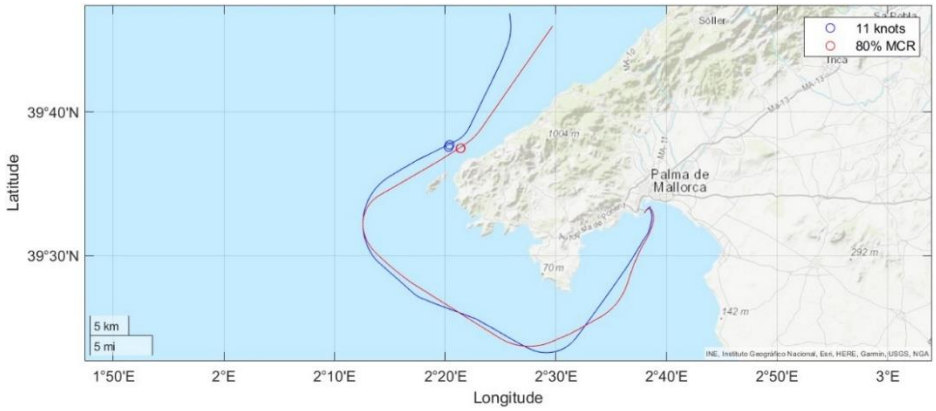

Figure 10-3 - Measurement locations for the far field measurements.

10.3 Post-Processing and results

10.3.1 General

The hydrophone measurements were processed according to the DNV class guideline DNV-CG-0313. The applicable time windows used for processing is based on the following expression:

$$time\ window = 2 * \frac{ship\ length}{ship\ speed}$$

For the bottom-mounted hydrophone, the DNV Silent class rules specify a -5 dB sea bottom correction and a general distance correction of $18log_{10}(r)$ where *r* is the distance from the vessel to the hydrophone at the closest point of approach (CPA) (ref. /4/).

$$URN = L_P + 18log_{10}\,(r) - 5\,dB$$

The SPL is corrected for the distance from the hydrophone to 1 m from the source, and eventually the results from the different hydrophones and runs are averaged on power basis to form the final result at each 1/3 octave band. In the current work carried out for the calibration measurements, there is only 1 run for each speed which simplifies the averaging to only apply between the various hydrophones.

10.3.2 Results 11 kn Quiet operating condition

During the measurements of the first run at 11 kn, the recorded operating conditions are presented in Table 10-3. Corresponding measured underwater radiated noise is presented in Figure 10-4, for the two bottom mounted hydrophones. The deviation between the two hydrophones at frequencies below 40 Hz is believed to be caused by measurement artefacts from movements in the hydrophone support structure.

The recorded operating conditions during the 11 knots measurement are presented in Table 10-3.

Table 10-3 - Operating conditions as recorded by CMX/NMEA data during the measurements.

Unit	Speed [rpm]	Power [kW]	Angle [Degrees]	Speed [kts]
Centre Line	50.5	1.120	-1.5	N/A
Starboard	50.0	1.120	-1.5	N/A
Vessel	N/A	N/A	N/A	11.2

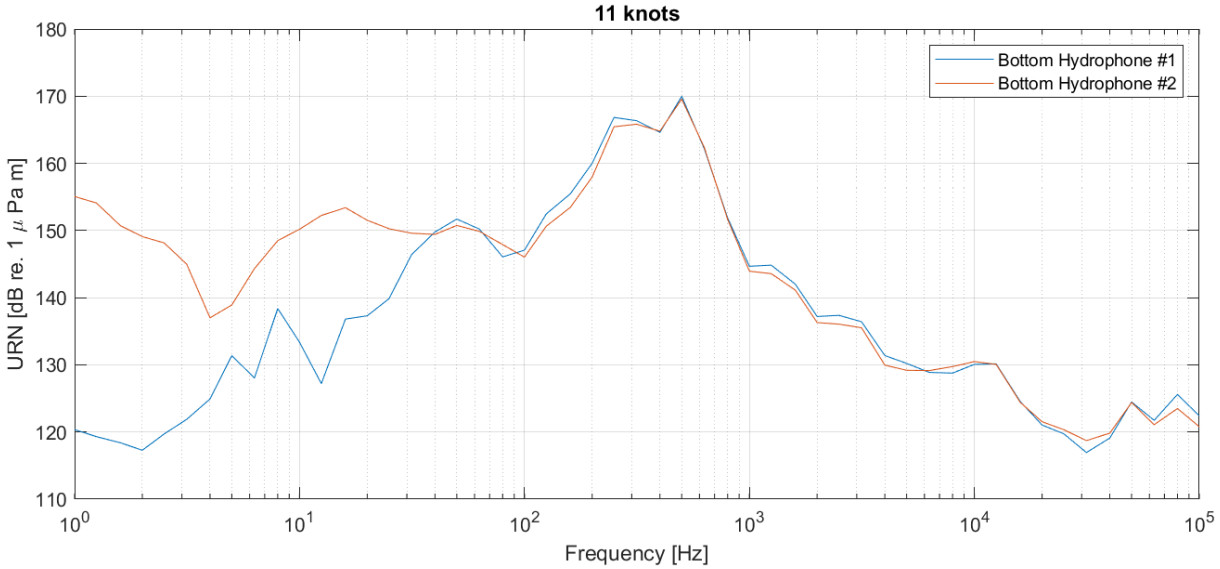

Figure 10-4 – Hydrophone measurement results for the 11 knots condition.

10.3.3 80% MCR

During the measurement of the 80% MCR condition subject to testing, three hydrophones were deployed; two were located on the seabed while the third was located at 18 meters below the free surface at the same horizontal location as bottom mounted hydrophone #1. The recorded operating parameters during the measurement are presented in Table 10-4 and the corresponding results from the measurements are presented in Figure 10-5.

Table 10-4 - Operating conditions as recorded by CMX/NMEA data during the measurements.

Unit	Speed [rpm]	Power [kW]	Angle [Degrees]	Speed [kts]
Centre Line	115	12.900	-1.5	N/A
Starboard	110	12.900	-1.5	N/A
Vessel	N/A	N/A	N/A	21.9

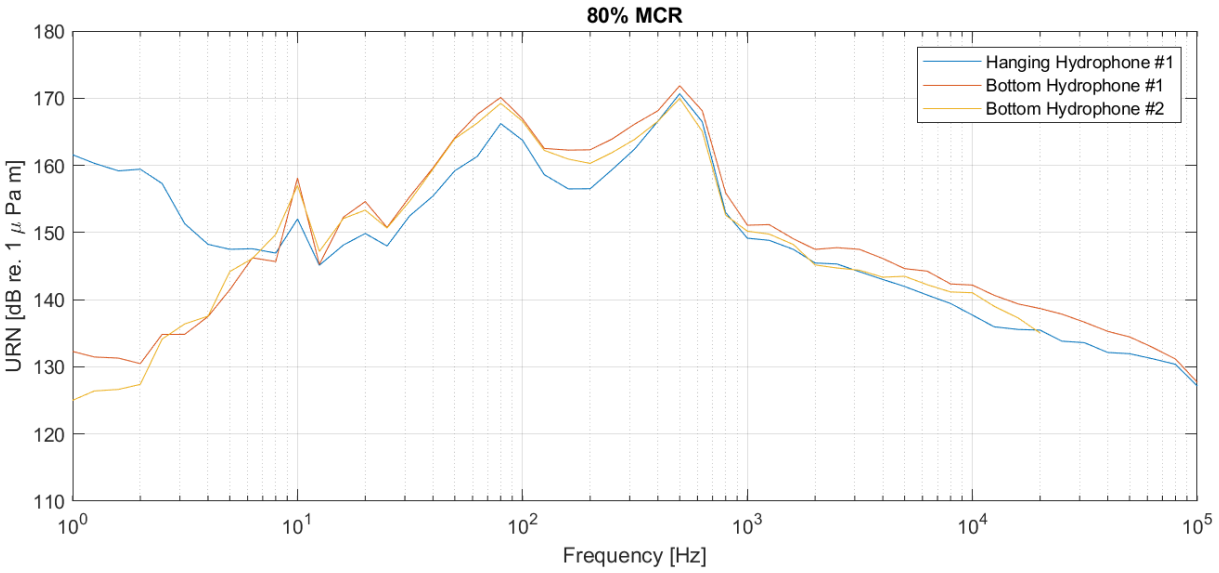

Figure 10-5- Hydrophone measurement results for the 80% MCR condition.

The agreement between the three hydrophones is considered as good. However, at frequencies below 8-9 Hz artefacts from the hanging hydrophone are evident. This is very typical for hanging hydrophones and are most likely resulting from current and wave induced motions of the hydrophone.

When comparing the two operating conditions, the measurements show fairly similar noise levels in the 500 Hz range which is dominated by electromagnetic noise. While the broadband noise floor is generally increased across a wider frequency range for the 80% MCR condition.

10.4 Comparison, far field vs onboard measurements

To compare the measurements in the near and far field, figures including the pressure sensors and one of the hydrophones are presented in Figure 10-6 and Figure 10-7 for the 11 knots (Quiet) and 80% MCR (Transit) conditions respectively. Please note that what is noted as pressure sensor measurements is corrected to what is defined as apparent far field radiated noise levels, see Chapter 5.1.1. This means that they are subject to corrections due to the time average effect of Lloyd mirror and solid boundary factor.

Most evident are the differences in the 60 and 80 Hz bands together with the deviation in the 500 Hz band between the two measurements methodologies. However, when comparing the measured far field URN levels of the two operating conditions, the measurements show fairly similar noise levels in the 500 Hz range which is dominated by electromagnetic noise. On the contrary, the broadband noise floor is generally increased across a wider frequency range between the two operating conditions for both measurement methodologies (similar trend).

The differences are better understood when studying the results with higher resolution as presented on the next page.

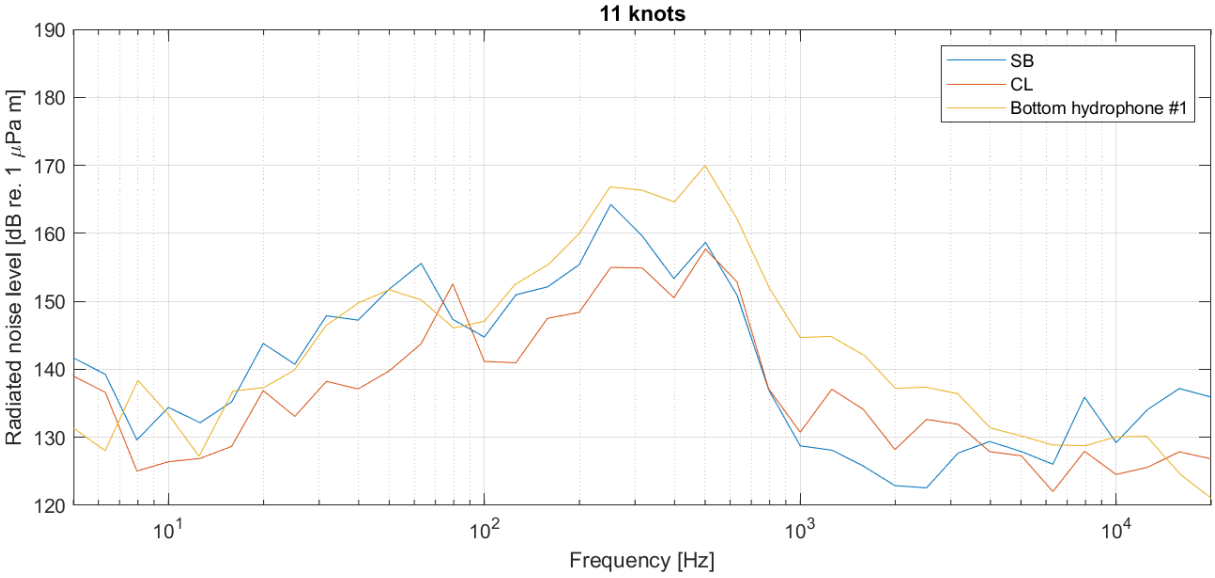

Figure 10-6 - 1/3 octave band comparison between near- and far field for the 11 knots condition.

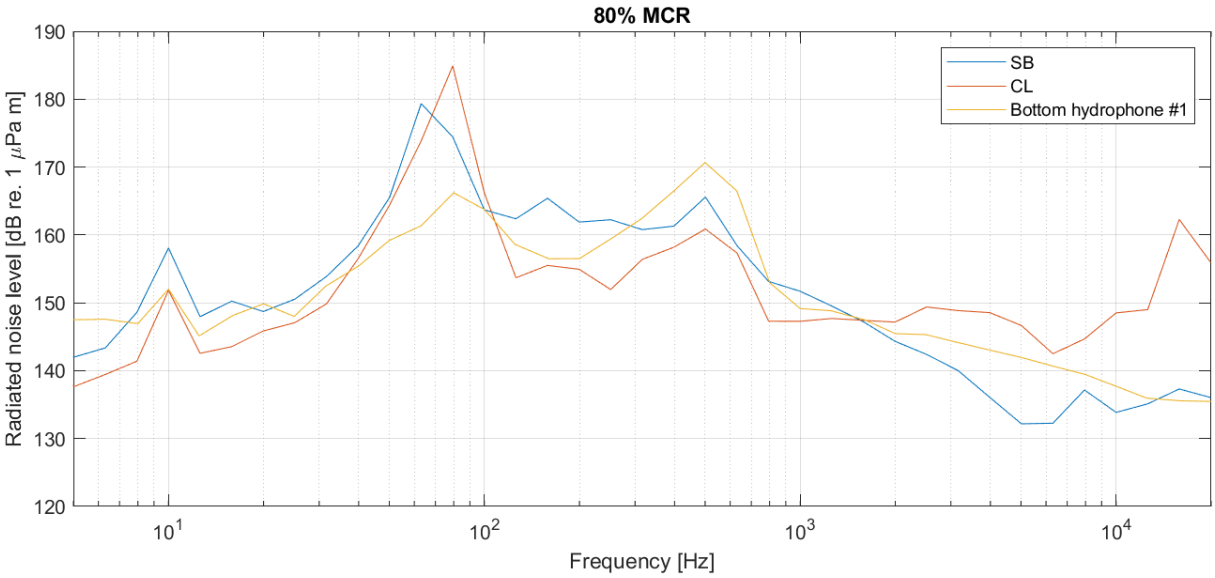

Figure 10-7 - 1/3 octave band comparison between near- and far field for the 80% MCR condition.

For a closer comparison of the different components and the difference between the measured levels by the pressure sensors and the hydrophones in the water column narrowband plots are provided below in Figure 10-8 and Figure 10-9 for the 11 knots and 80% MCR conditions respectively.

One of the main differences between the results obtained from the pressure sensors and hydrophones is the capability of characterizing the radiated noise levels from the diesel generators. Four-stroke diesel generators are generating noise at each half order of the rotation rate. From the spectra at each operating condition, the main contribution from the diesel generators can be identified as tonals, at 5 Hz and multiples of 5 Hz. Due various factors, among them the distance from the pressure sensors to the diesel generators as well as the size of the effective source (size of the ship), these are not well characterized by the onboard pressure sensors. As long as the diesel generators are resiliently mounted, it is not expected that the contributions from the diesel generators will cause excessive noise levels when comparing to the criteria of a typical underwater noise notation from DNV or similar. It is however recognized that this is one of the apparent differences between the measurement methodologies, but is not pursued in further detail due to the reasoning above. The amplitude of the blade passing frequency from the propeller, as well as its harmonics are also significantly more pronounced in the signal from the pressure sensors. This is due to poor radiation efficiency and is explained in more detailed in Chapter 9.4.

When comparing the results in the range between 60-80 Hz, two components are visible in the pressure sensor data and not in the far field hydrophone data. Based on experience from previous vessels, this is likely a singing phenomena occurring close to the pressure sensors. The reasons for not going further into the details of this phenomenon is further discussed in Chapter 9.4. However, by comparing the measurements in the near and far field, it is quite obvious that the radiation efficiency of the phenomenon is poor. In the higher frequencies, it can be seen that the pressure sensors underestimate some frequency components, including the noted electromagnetic noise at around 500 Hz.

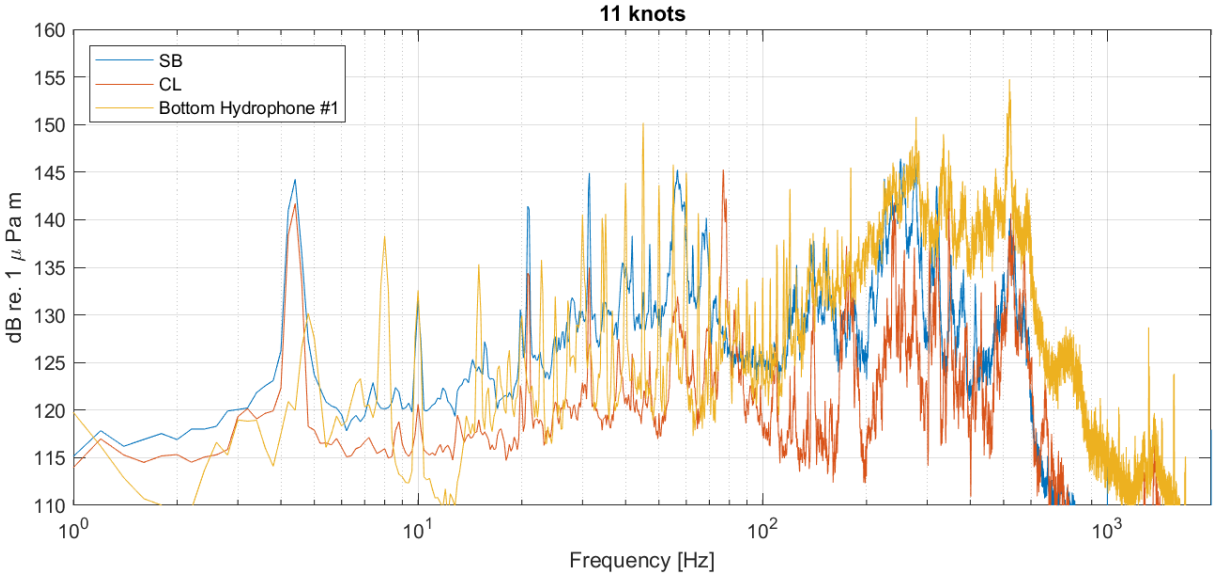

Figure 10-8 - Narrowband comparison between near- and far field for the 11 knots condition.

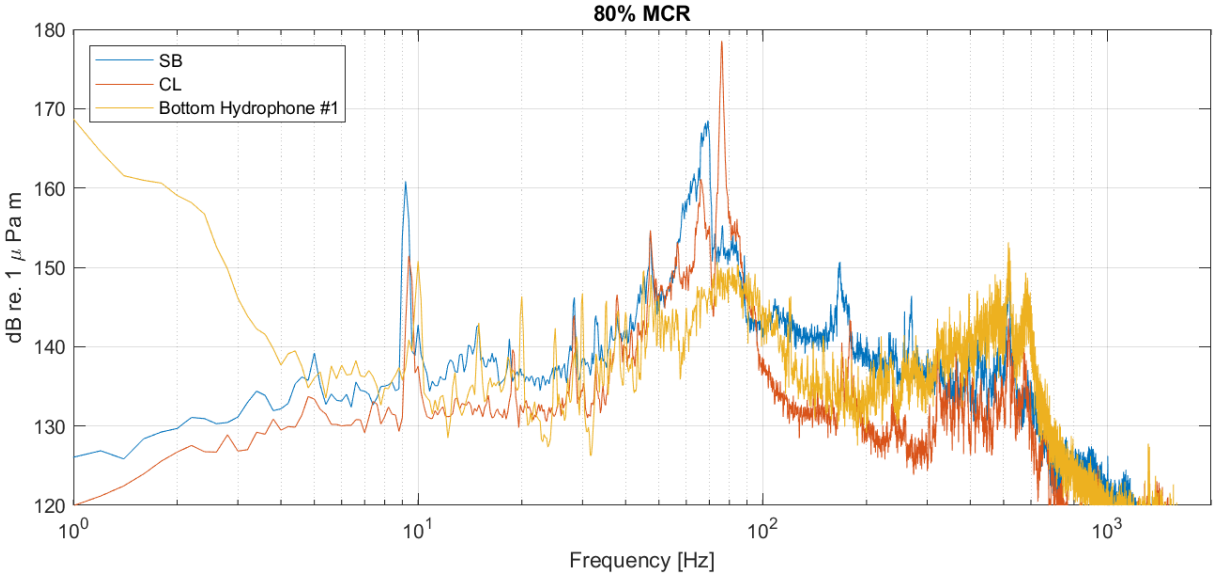

Figure 10-9 - Narrowband comparison between near- and far field for the 80% MCR condition.

10.5 MURN Estimator

The main deviations between the near and far field measurement methodologies are caused by differences in characterisation of magnetic noise. As expected, the magnetic noise component needs correction/MURN-adaptation to match the far-field results to a satisfactory extent.

In theory, both methods should produce similar results for URN and if they fail to do so, then the differences might be because the near-field sensor is not capturing the magnetic noise signature accurately. Therefore, an accelerometer was added to SB and CL pod stator to “augment” the near-field method for better accuracy, see Figure 3.

The methods for magnetic noise estimation presented earlier were applied to the measured vibration to improve the magnetic noise detection accuracy of the near-field method.

The measurements were carried out for two vessel operation conditions:

1. Vessel speed 11 kt (Quiet Cruise condition for DNV Silent-E), SB and CL pod: 50 and 50.5 RPM.
2. Vessel speed 20 kt or 80 % MCR (Transit condition for DNV Silent-E), SB and CL pod: 110 and 115 RPM.

10.5.1 Quiet Cruise results

Vibration correction /adaptation was applied to the measured vibrations and the adapted MURN was then estimated based on the weights obtained from the correction. The corrected near-field URN is shown in Figure 16. The near-field total source level (black curve) was obtained by adding together the sound pressures from each propulsor (two SB propulsors and one CL propulsor):

$$L_{S,Total} = 20\log_{10}\frac{\sqrt{2{p_{SB}}^2+{p_{CL}}^2}}{p_{ref}} \quad (18)$$

, where $L_{S,Total}$ is the total propulsion source level and p_{SB} and p_{CL} are the SB and CL propulsor sound pressures in units of Pascals.

In an ideal world the black and blue curve should be similar, which in this case does not occur. This is where the MURN adaptation is needed since in the frequency range 315-2500 Hz the magnetic noise dominates the noise emission, but the pressure sensor does not capture the magnetic noise well enough. If only the simulated MURN is used (red curve), one ends up having an overestimated MURN, which can be avoided if the MURN is corrected using the measured stator

vibration. The corrected source level is obtained by replacing those parts in the measured near-field source level, where corrected magnetic noise dominates the response.

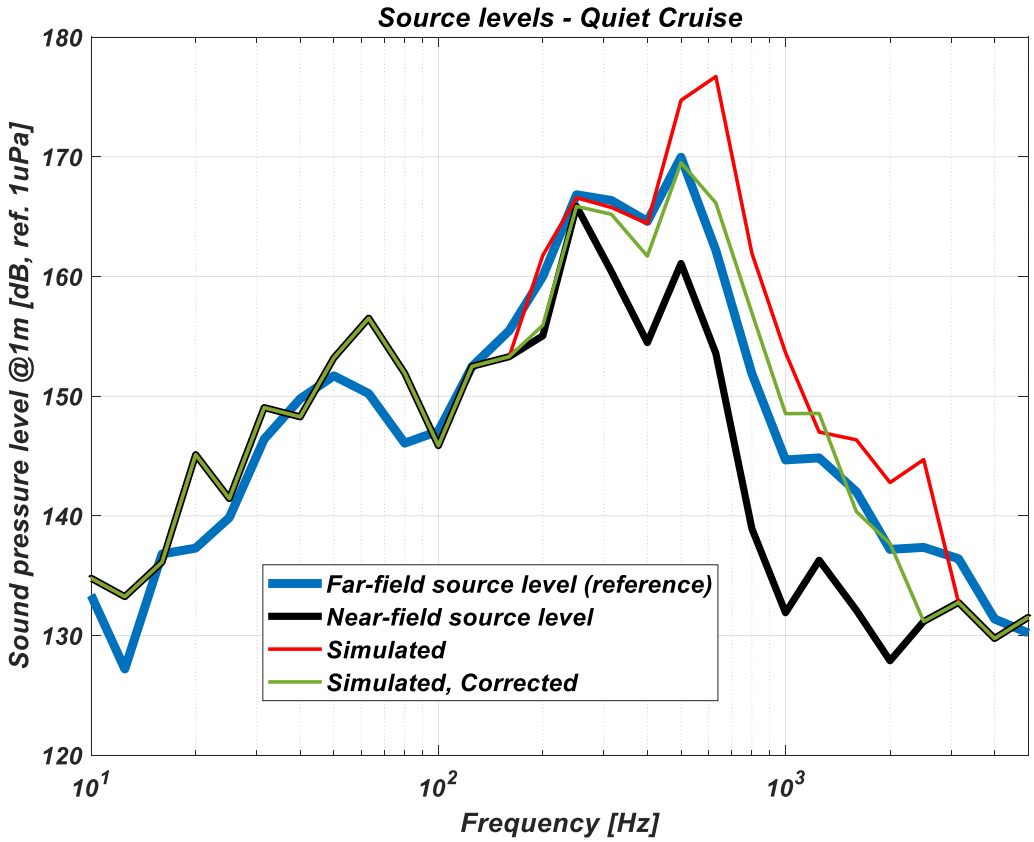

Figure 10-10 - Measured and simulated vessel underwater radiated noise levels during a quiet cruise condition.

10.5.2 Transit results

The corrected near-field URN is shown in Figure 10-11. The near-field total source level (black curve) was obtained by adding together the sound pressures from each propulsor using Eq. 18.

In an ideal world the black and blue curve should be similar, which in this case does not occur. This is where the MURN adaptation is needed since in the frequency range 315-2500 Hz the magnetic noise dominates the noise emission, but the pressure sensor does not capture the magnetic noise well enough. If only the simulated MURN is used (red curve), one ends up having an overestimated MURN, which can be avoided if the MURN is corrected using the measured stator vibration. The corrected source level is obtained by replacing those parts in the measured near-field source level, where corrected magnetic noise dominates the response.

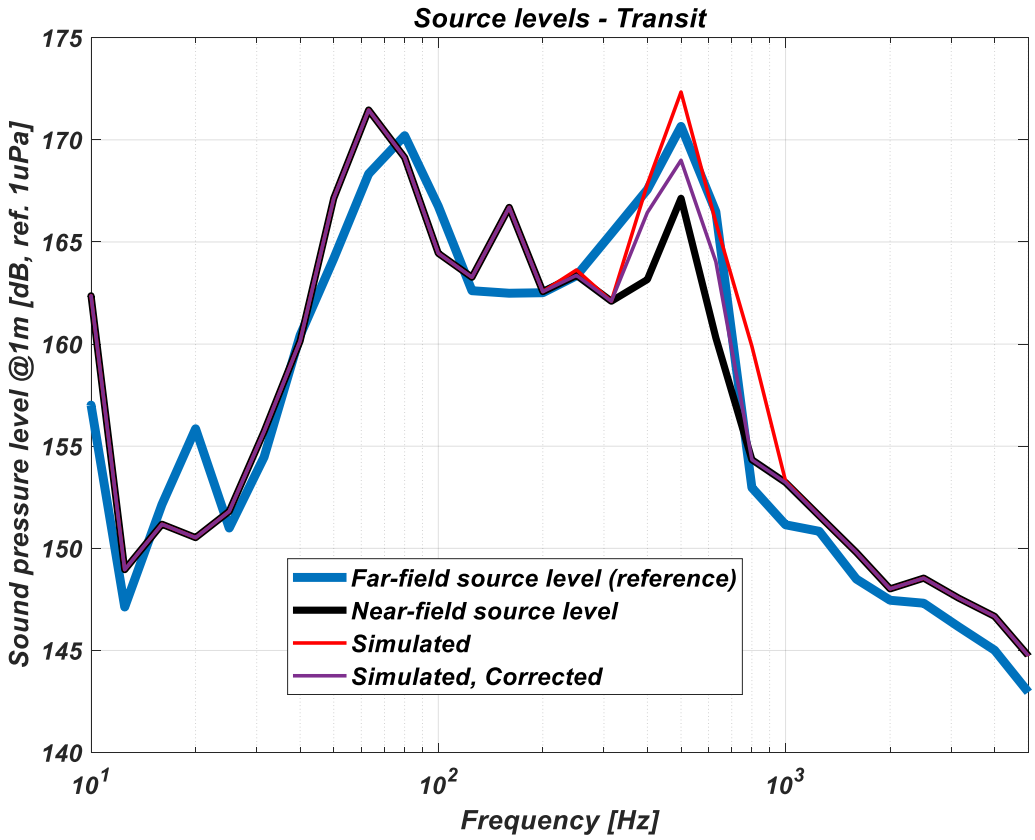

Figure 10-11 - Measured and simulated vessel underwater radiated noise levels during a transit condition.

11 REFERENCES

/1/	PADVT-QVI-CONTRIBUTION AGREEMENT-DNV AS_2023	20-03-2023
/2/	Final Proposal - QVI-IndustryAcademia-CLUE_DNV_ABB	30-06-2021
/3/	TN23-27 CLUE Progress Report Fiscal Year 2022-2023	31-03-2023
/4/	DNV-CG-0313 – Measurement Procedures for Noise Emissions	July 2022